ABSTRACT

Title of Document:	USING INVERSE FIRE MODELING WITH MULTIPLE INPUT SIGNALS TO OBTAIN HEAT RELEASE RATES IN COMPARTMENT FIRE SCENARIOS. Michael D. Price, Masters of Science 2014
Co-Directed By:	Dr. Arnaud Trouvé and Dr. Andre Marshall, Fire Protection Engineering

A set of multi-room compartment fire experiments were conducted to obtain measurements of hot gas layer temperature and depth. These measurements were used as an input to an inverse fire model that coupled a genetic algorithm with a zone fire model to calculate a unique solution to the original fire size and door opening used in the experiments. The objective of this research was to calculate simultaneously the real-time fire size and fire door opening of the experiment using a combination of hot gas layer temperature and hot gas layer height measurements from a multi-room compartment in concert with an inverse fire model. This research focused on increasing the robustness of an inverse fire model (IFM) with respect to physical accuracy and multi-variable calculations. The IFM successfully identified a unique solution and calculated fire size within 10-40% of experimental values.

USING INVERSE FIRE MODELING WITH MULTIPLE INPUT SIGNALS TO OBTAIN HEAT RELEASE RATES IN COMPARTMENT FIRE SCENARIOS

By Michael D. Price

Thesis submitted to the Faculty of the Graduate School of the
University of Maryland, College Park in partial fulfillment
of the requirements for the degree of
Masters of Science
2014

Advisory Committee:

Professor Andre W. Marshall, Chair
Professor Arnaud Trouvé
Professor James Milke

Acknowledgments

I would like to acknowledge and thank the following people who have helped me throughout this process.

First, I would like to acknowledge and thank Dr. Milke going back to 2008, when he helped me in the initial stages of forming a Gemstone undergraduate research team that launched my involvement in the field of Fire Protection Engineering. Even from New Zealand, and with scant time to offer, he provided me with critical insights into the merit of the proposed research topic, which ultimately transformed itself in the six months following its conception. From then he was always warmly responsive to both me and my team for the next three years of undergraduate research, even though not a single student in the team was from the FPE department.

I would also like to acknowledge and thank Dr. Marshall for providing me this opportunity to be in the Masters program in the FPE department. It was Dr. Marshall who provided an opportunity to continue working in research areas directly related to the Gemstone work that “ignited” my passion for the field. He also gave me the opportunity to contribute to preparation for the SNIFFR NSF ERC project, a research effort that constitutes the ultimate goal of what my Gemstone project aimed to build one part of.

I would like to recognized and thank Dr. Trouvé for his many contributions, above all for his patience as he guided a student he may not have expecting to introduce to the field of inverse modeling. He took a great deal of his very valuable time to help, teach, and direct me through various stages of the research project, helping to shape the

direction that needed to be taken at various steps when significant problems and challenges arose. Dr. Trouvé's support has been critical to the success of my thesis work.

I would also like to thank the Dr. Darryl Pines, Dean of the Clark School of Engineering for the seed funding they provided in support of this research.

I would like to express my sincere thanks and gratitude to Pat Baker. For several years she has helped me at every turn without hesitation, whether to make sure I had the proper paperwork to enter the MS program, answer any and every question, to knowing where a key professor might be found.

Sharon Hodges watched out for me when I didn't even know I was not correctly registered for classes.

I would like to my thanks to my brother James Price for always being willing to provide advice and support to my programming challenges. As a professional computer engineer of five years, he had a lot of insight to provide. My code may never have worked quite as well without his assistance.

Finally, I would like to thank Nicole Hollywood and Dianne Barrett, without whom none of this defense would be possible.

Table of Contents

Table of Figures

Table of Tables

Chapter 1: Introduction

1.1 Context

Fire costs over $300 billion a year in the U.S. [1]. This cost includes injuries, death, damage done to property, fire departments and volunteer firefighters. Fires are damaging because they can develop rapidly causing considerably more damage over time. If Emergency First Responders (EFRs) could respond more quickly and precisely to a fire by knowing its size and location within a building then fire cost could be reduced. Currently, EFRs do not have real-time access to the size and location of a fire. However, with a combination of new building technologies and computational methods this information can be calculated and provided to EFRs in real-time.

In this study, an approach to calculating real-time fire information for EFRs was explored. To this end, a set of multi-room compartment fire experiments were conducted to obtain measurements of hot gas layer temperature and depth. These measurements were used as an input to an inverse fire model that coupled a genetic algorithm with a zone fire model to calculate a unique solution to the original fire size and door opening used in the experiments.

1.2 Literature Review

A variety of methods for calculating fire information based on measurements have been attempted in past research. Typically the process utilizes an inverse fire model.

Traditional fire modeling, or "forward" modeling, takes a set of initial conditions such as fire size, fuel, room geometry, construction materials, and many others, and calculates the impact of the fire on the environment. Conversely, an inverse fire model takes resulting conditions, such as the temperature rise, and seeks to determine what initial conditions created that result. Inverse modeling allows for measurements of the environment to be assimilated into a model to determine original fire conditions and use that knowledge to forecast the size and location of the fire further into an emergency. Inverse modeling has been used from small-scale fires, to compartment fires, all the way up to wildland fire scales. The following sections discuss previous work in the area of small scale and compartment fire modeling as well as wildland fire forecasting that led to this research effort.

1.2.1 Small-scale Inverse Fire Modeling

A number of studies have been done with small-scale fire configurations. Cowlard et al. examined the use of data assimilation techniques with small-scale vertical flame spread of PMMA plastic [2]. Their research used a series of thermocouples and a Particle Image Velocimetry (PIV) system with two video cameras to measure the spread of fire along a 200 mm vertical slab of PMMA and simultaneously predict future spread with the Fernandez-Pello model for vertical flame velocity. The measurements from the thermocouples and cameras helped refine variables in the model that change with time and the model was updated to more accurately predict fire growth. The forecasting of vertical flame spread became significantly more accurate the longer the PMMA burned.

Lautenberger et al. worked on performing predictions on the material properties of pyrolyzed solids using a Computational Fluids Dynamics (CFD)-based fire growth

modeling from bench-scale fire test data [3]. This approach used the FDS v4.0 solid pyrolysis model for a more mathematically robust approach to burning fuel calculations. The pyrolysis model was combined with a genetic algorithm (GA) to estimate the material properties for fire growth based on cone calorimeter data of the burning materials. GAs are effective at handling nonlinear problems and high dimensionality. As a result, the GA successfully optimized what physical materials were used in a modeled solid fuel pyrolysis by identifying what physical properties of the burning material must have yielded the model's predictions. GAs have been used in other fire modeling research such as predicting the kinetics of polyurethane foam combustion. Rein et al. Discusses the practical use of GAs in fire inverse modeling.

1.2.2 Compartment Fire Modeling

Lee and Lee have also studied inverse fire modeling to calculate heat release rates by use of a sequential inverse method [4]. Pairing an optimization algorithm focusing on the sequential regularization approach with the Fire Dynamics Simulator (FDS 82), an estimate of the location and size of the fire can be calculated using temperature measurements along the ceiling inside a compartment. The research compared temperature profiles inside a compartment to predictions from an FDS model of the compartment. By minimizing the residuals between measured and predicted values, the location and heat release rate of the fire were calculated.

Davis and Forney developed the National Institute of Standards and Technology's Sensor-Driven Fire Model (SDFM) to calculate fire size [6][7]. The SDFM employs ceiling-jet correlations with sensor measurements to approximate heat release rates (HRR) of fires. These HRRs are provided to a CFAST model of the building that the fire

takes place in. CFAST then makes predictions of HRR growth, hot gas layer temperatures, smoke/visibility concerns, and even predict structural failure. CFAST is a zone fire model that performs more simplified calculations than a full scale CFD model. As a result, it is computational inexpensive and fast.

FireGrid aimed to perform super-real time modeling of building fires while the fire was occurring [8]-[10]. The FireGRID process explored a variety of methods for super-real-time modeling. One approach utilized a coupled simulation tool based on the Monte-Carlo-based fire model, CRISP. The project used measurements from full-scale compartment fire experiments undertaken in Dalmarnock, Glasgow in 2006. A six-room experiment, the compartment was instrumented with temperature, heat flux, optical density, gas velocity and structural monitoring sensors. Data from these experiments served as pseudo-sensor input data for the CRISP model. CRISP employed a two-layer zone model with a detailed model of human behavior and movement. The Monte-Carlo approach randomized the input data and ran one thousand simulations. The results of these simulations are then compared to the measured data and a best fitting model is determined. The heat release rate and burning properties prescribed to that model are then taken as the answer to the experimental HRR. FireGrid also explored taking data from numerous building sensors to obtain temperature, smoke, and CO measurements to plug into a simultaneous CFD and Finite Element models. This approach was able to calculate not only fire size and location, but also the impact the fire had on the structure. Ultimately, the FireGrid approach was too computationally expensive to achieve its super-real time goals.

1.2.3 Wildland Fires Forecasting

Rochoux et al. employed meteorological data assimilation techniques often used in weather forecasting for wildland fire forecasting [11]-[14]. The approach used is similar to the genetic algorithm approach; an optimization calculates the best possible solution out of a set of models compared to a variety of sensor measurements that displays the actual real-time result. Instead of using a genetic algorithm, a Kalman and subsequently an ensemble Kalman filters are used. The Kalman filter was a more computationally efficient optimization algorithm than a GA. The algorithm begins with an initial guess of the control parameters while a forward model produces prediction of the wildland fire front location. The model prediction is compared to the sensor observations of the physical location of the fire front. The deviation between the prediction and observation produces an analysis vector that serves as a correction factor. The Kalman filter could serve as a future upgrade to the IFM used in this research.

1.2.4 Prior Inverse Fire Model Development

In 2007 Neviackas developed the Inverse Fire Model (IFM) used in this research [15]. The goal of the experiments conducted was to prove the concept that given a temperature of a hot gas layer over a function of time, that the heat release rate of the associated fire could be determined. Using a Matlab-based GA and Windows batch files to run the zone fire model BRI2002, Neviackas developed an IFM that read input temperature signals and ran a barrage of BRI simulations aiming to find what sized HRR could best replicate this signal. In the experiments, Neviackas used a synthetically-generated reference temperature curve as the input signal, using either BRI or FDS to generate the signal. Neviackas did work on a variety of different configurations, ranging

from 2 to 20 rooms, with a variety of fire sizes, ranging from hundreds to thousands of kilowatts. Neviackas' results were promising. The IFM consistently obtained HRR very close to the actual reference values, generally within ~10% and often on the order of ~1%. However, when Neviackas set the ventilation conditions (the size of the doors and windows in any given room) to be another variable alongside the heat release rate, the solution space of the IFM became non-unique; there were now multiple different combinations of fire size and door widths that could produce the same temperature curve.

The problem of non-uniqueness in this problem set can best be understood by looking at the McCaffrey, Quintiere, and Harkleroad (MQH) correlation that shows the relationship between the temperature of a hot gas layer and the size of the fire and the physical parameters of the compartment. The MQH correlation is shown below:

$$\Delta T_g = 6.85 \left(\frac{\dot{Q}^2}{A_0 \sqrt{H_0} h_k A_T} \right)^{\frac{1}{3}} [16]$$

Where ΔT_g is the change in hot gas layer temperature, $\dot{Q}$ is the heat release rate of the fire, A_0 is the area of the vent opening out of the fire room H_0 is the height of the opening, h_k is an effective heat transfer coefficient, and $A_T$is the total area of the enclosure around the fire. In the above equation, it can be seen that by decreasing both the area of the vent, by either height, width or both, and decreasing the HRR in a proportion to that vent change, the change in hot gas layer temperature remains the same. This proportion is where the problem of non-uniqueness occurs.

Thus the problem of uniqueness occurs in Neviackas's research. Depending on the scenario, its environmental conditions, and the fire condition, non-unique IFM results

could be very different from the actual correct result. Sometimes, the IFM would settle on the correct solution but many times it would not [15]. The IFM had to guess the widths of many doors in the 20-room scenario and it rarely chose them correctly. In many cases choosing the door sizes did not affect the final results, as only the one door directly letting out from the fire room had a large impact on the temperature profile. However, many times the width of the fire room door opening was incorrectly identified, and the subsequent heat release rate was not correct. Instead of answers within 1%-10% of the reference values, values could be off by as much as 10%-50%[15].

Unfortunately, while the IFM is accurate more often than not, the multiple-solution occurrence poses a significant problem. EFRs require tools that are completely reliable. As long as multiple solutions exist, there is no guarantee that the IFM will find the correct solution. If the multiple solutions are significantly different from the correct solution and is reflected by the IFM, inaccurate information could be provided to EFRs.

Many different approaches to calculating fire size in a building have been attempted. CFD based approaches are impractical given their high computational expense. Other approaches require too much knowledge of the fuel, or too close observation of physical phenomena in a building to be realistically obtained from building sensors. Finally, many assumptions are made in these models, many that may not be practical in real scenarios. The number of assumptions used in inverse fire modeling must be reduced to make the technique more broadly capable.

1.3 Objective

The purpose of this study was to explore the accuracy of the inverse fire model (IFM) in real applications. This research approaches the problem of multiple solutions using experimental data from a multi-room compartment fire scenario as the input to an IFM; previously the input data had been synthetically generated. The experimental data gathered was the hot gas layer temperature and depth.

Previous work has demonstrated that inverse fire modeling can calculate fire size through a variety of methods. However, these methods require too many assumptions that do not reflect real scenarios. While modern building infrastructure may allow for the construction materials and geometries to be known in advance of an emergency, the state of doorways is highly variable and not likely to be known. If this variable is not accounted for, then there are multiple possible solutions to the size of a fire. The objective of this research was to calculate simultaneously the real-time fire size and fire door opening using a combination of hot gas layer temperature and hot gas layer height measurements from a multi-room compartment in concert with an inverse fire model. The method of using two measurement inputs to attempt to find a unique solution in the event that door conditions are not known is a novel approach to this problem.

Chapter 2: Approach

This research focused on increasing the robustness of the inverse fire model (IFM) with respect to physical accuracy and multi-variable calculations. The IFM was tested using experimental results instead of synthetically generated results from computer models. Multiple variables were used from these experiments to aid the IFM in finding a unique solution in a multi-variable problem where fire size and fire room door width are unknown. The experiments were originally conducted to examine how environmental sensors, more numerous than fire sensors in modern construction, "saw" fire. However, these environmental sensor measurements were not used in the IFM calculations and will not be discussed in this paper. Thermocouple measurements were taken alongside the environmental sensor measurements. These thermocouple measurements of the hot gas layer are required for use with the established IFM. In order to improve the robustness of the IFM, these measurements included not only the temperature but also the approximate depth of the hot gas layer. By using these two different variables together, the IFM was able to handle a multi-variable problem and identify a unique solution.

This study was composed of two phases. Phase one was a multi-room compartment fire experiment. Phase two was a simulation phase using measured data obtained from the experiments.

2.1 Compartment Fire Experiment

The compartment configuration, seen below in Figure 2-1, contained two adjacent rooms connected by a corridor room. The fire room was designated Room 1, the corridor was Room 2, and the adjacent room was Room 3. Both rooms were approximately 1.9 m

x 2.5 m. The hallway was 3.65 x 1.1 m. The height of the whole structure was 2 m. The outer geometry of the compartment was limited by the fire hood size in the FireTEC fire lab.

The compartment did not have any vents leading to outside conditions. However, it did have holes in construction to allow for an obscuration laser to pass into/out of the compartment, as well as some construction leakages that led to visible smoke seen coming out of cracks in construction at some points during experiments. Leakage was seen most in Room 3 where an exit vent was established to help ventilate the compartment between experiments. The exit vent was shut during the course of all experiments.

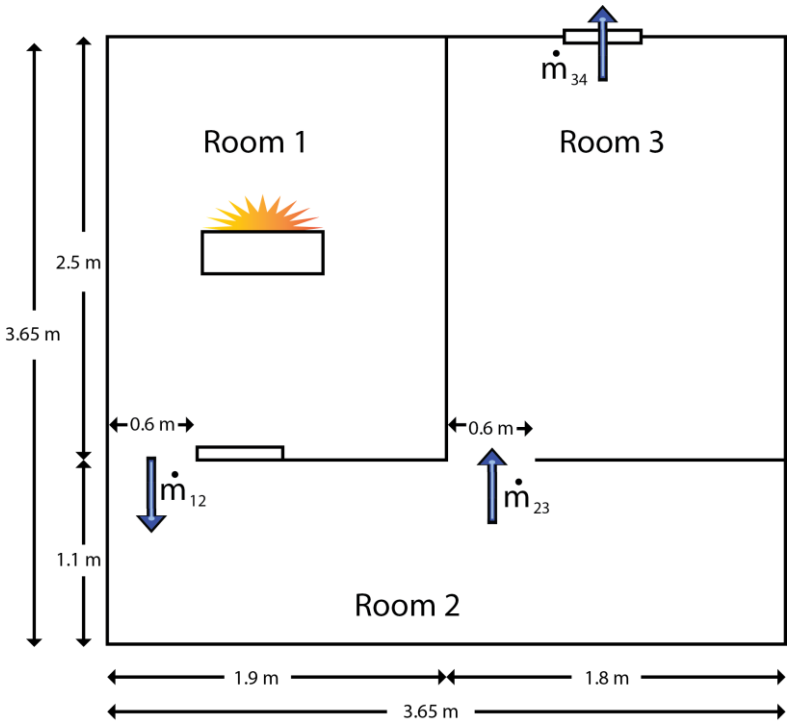

Figure 2-1: Three room experimental compartment with a gas burner in Room 1

The compartment was setup with a variety of instrumentation to gather data. Figure 2-2 shows the type and location of each measurement device. The gas sand burner was placed in the middle of Room 1. Each room was instrumented with four environmental sensors, two attached to the ceiling, two attached to the wall. Additionally, each room was instrumented with one thermocouple tree with ten evenly spaced k-type thermocouples. A laser obscuration measurement apparatus was setup to examine smoke obscuration in Room 1. Video cameras were installed in each room, with one lamp in each room to provide visibility. One smoke detector and sprinkler head were placed in each room to track their activation times during the experiments. Experiments were run at steady fire sizes ranging from 5 kW to 50 kW with run times of 2.5 to 10 minutes. The duration of the experiments was based on hand calculations of when the hot gas layer would descend to the burner, possibly interfering with the combustion process and making the fire unsteady. The fuel used was propane gas. Steady fires were employed because this study not only seeks to be the first comparison of the IFM with experimental results but also establish the entirely new feature of using multiple input signals, dramatically increasing the complexity of the problem.

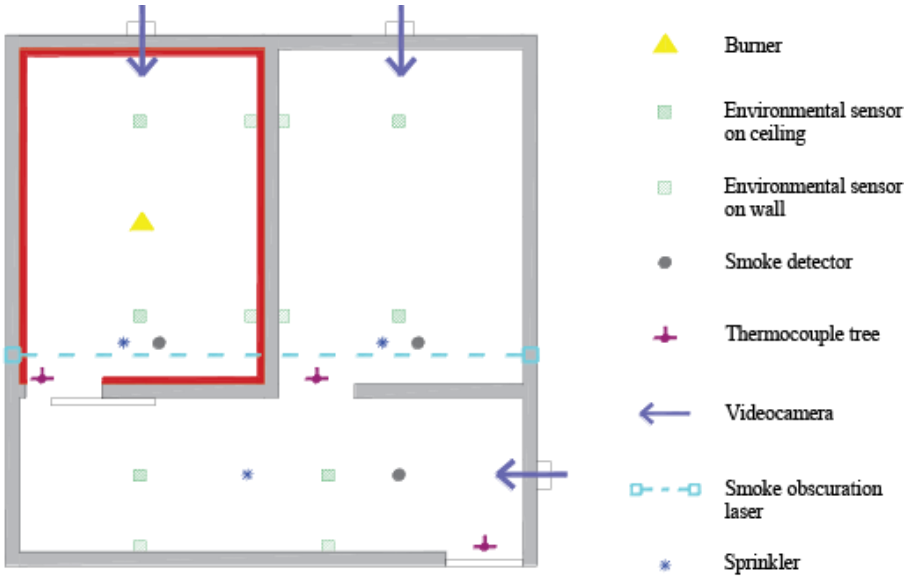

Figure 2-2: Sensor location in experimental configuration [17]

This experiment allowed for the temperature of the gases in the compartment to be measured over the course of the experiment at 10 different evenly spaced heights. The spatial data from these thermocouple measurements were used for calculations of the hot gas layer height and hot gas layer temperature for input into the second phase.

2.2 Phase 2: Inverse Fire Model Simulation

The IFM simulations require properly prepared input data, a selected zone fire model, and a genetic algorithm in order to calculate fire size.

2.2.1 Input Data

In order to convert the discrete temperature measurements into an average hot gas layer temperature a stratification temperature was needed to mark where the transition from cold lower layer to hot upper layer occurs. This stratification temperature was determined using methods from NFPA 92. Using equations 5.5.1.1 (d) and (e) for the

mass flow from an axisymmetric plume with equation 5.5.5 for the temperature of a hot gas layer, the stratification temperature for a 50 kW fire was calculated [18]. These equations and results are shown below.

Eq. 5.5.5 [18]: $T_s = T_0 + \frac{K_s Q_c}{m C_p}$

Eq. 5.5.1.1 (d): $z_1 = 0.166 Q_c^{2/5}$

Eq. 5.5.1.1 (e): $m = \left(0.071 Q_c^{1/3} z^{5/3}\right) + 0.0018 Q_C$ when z > z_1

Where T_s is the smoke layer temperature in C, T_0 is the ambient temperature in C, K_s is the fraction of convective heat release contained in smoke layer (assumed to be 1), Q_c is the convective portion of heat release rate in kW(assumed equal to 0.7*HRR), m is the mass flow rate of the plume at height z in kg/s, C_p is the specific heat of plume gases (1.0 kJ/kg-C), z_1 is the limiting height in m, and z is the distance between the base of the fire to the smoke layer in m. Given a 50 kW fire size, the convective portion of the HRR is 35 kW. The base of the fire is approximately 20 cm from the floor of the 2m compartment, so when the smoke layer is first forming, z is = to 1.8 m. Plugging 35 kW to calculate $z_1$yields 0.56 m, thus Eq. 5.5.1.1 (e) applies. Solving for the mass flow rate yields 0.55 kg/s. Plugging the mass flow rate into Eq. 5.5.5 yields a temperature of 69.87 ºC, which was then rounded to 70 ºC for convenience.

It should be noted that these equations from NFPA 92 use an adiabatic estimate for the plume temperature at the height of the smoke layer interface, but this assumption is not valid in the experimental scenario. Because the compartment is very small, there are more significant thermal losses through the walls that would otherwise not be observed in the larger compartments or atria that the equations are typically prescribed

for application. Additionally, the threshold temperature actually changes as a function of time, thus using a single temperature to represent the stratification is an approximation used for simplicity. Another approach to determining stratification could be to not assume knowledge of K_s, the fraction of convective heat release, and actually try to calculate value from the experimental data. If the threshold temperature were changed, different results could be obtained from the IFM. In fact, a lower temperature threshold of 60 degrees C allows for more accurate fire size calculations.

As the hot gas layer descends and each thermocouple reaches the stratification temperature, the height of that thermocouple is noted, and the average hot gas layer temperature is calculated as the spatial average of all temperature measurements above that point where each thermocouple measurement is approximated as representing the average temperature of the space above the thermocouple until reaching the next thermocouple on the tree. This approximation provides both the temperature over time of the hot gas layer as well as the depth, where the depth is linearly interpolated between each time that a new, lower, thermocouple reaches the stratification temperature.

2.2.2 Zone Fire Model Baseline

The zone fire model used in this research was the same one used in Neviackas, BRI2002 (BRI). BRI was designed by the Building and Fire Research laboratory in Tsubaka, Japan. BRI was selected over another established zone model developed by NIST, CFAST, due to BRI's higher numerical stability across a large range of fire sizes. The GA approach used in the IFM requires hundreds to thousands of simulations to be run. CFAST crashed on a large range of these tests, causing too many failures to allow the GA to properly converge.

As a zone model, BRI performs calculations using a set of assumptions show below:

i. “Any space in a building is filled with an upper and a lower gas layer
ii. The upper and lower layers are distinctly divided by a horizontal boundary plane (discontinuity)
iii. Each layer is uniform with respect to physical properties by virtue of vigorous mixing
iv. Mass transfer across the boundary of a layer occurs only through a fire plume, doorjets and doorjet plumes
v. Heat transfer across a layer boundary occurs by radiative heat exchange among the layers and the boundary surface contacting with the layer, as well as that associated with the mass transfer referred in (4)
vi. All the heat released by a fire source is transported by the fire plume, in other words, the flame radiation loss is neglected.” [19]

As a result of these simplifying assumptions, there will be some discrepancy between the experimental fire measurements and the BRI results. A simulation of the experimental scenario with the complete construction geometry and steady 50 kW fire was run to establish a baseline for expectations; specifically, the baseline simulation demonstrated if BRI accurately reflects the experimental results or if it will under or over predict.

BRI does not allow for a compartment that has no vent to outside conditions. To attend to this requirement, a vent was added in Room 3 to represent the sum of both the leakages out of the third room and the opening for the laser sensor. The discrepancy between the actual experimental geometry and the simulation geometry was a source of error. The simulated fire size was a static 50 kW propane fire. Below is a sample BRI

input file representing the three-room scenario with a 50 kW propane fire and a fixed door width.

```
Compartment Fire
2013.11.20
01
SAMPLE_CALCULATION
    200        1.     100.0       1.0
    1
      2.00
    3
1 (FIRE ROOM)            1       0.0      2.00    1   27   27    1
       0.0      1.90      2.50
2 (HALL ROOM)            1       0.0      2.00    1   27   27    1
       0.0      3.70      1.10
3 (COLD ROOM)            1       0.0      2.00    1   27   27    1
       0.0      1.80      2.50
   1     2    1       0.5       2.0       0.0                    0
   2     3    2       0.5       2.0       0.0                    0
   4     3    3       0.3       0.3       0.0                    0
 9999
 9999
    1
    4    1
       0.0        30        60        90       120       150
       0.0        50        50        50        50        50
       0.0      0.08      0.08      0.08      0.08      0.08
       0.0       0.0       0.0       0.0       0.0       0.0
    4
    1    1
      22.0      50.0
    0
    1
      22.0      50.0
    2
       0.0      0.00      0.00
       0.0
    0
 9999
```

The BRI results of the compartment configuration produce the average hot gas layer temperature in time and the hot gas layer depth in time. Figure 2-3 shows the temperature over time produce by a 50 kW fire with a fixed 0.6 m door width. The BRI results show a development phase of rapid temperature rise while slowly the temperature increase slows down over the course of a 150 second experiment.

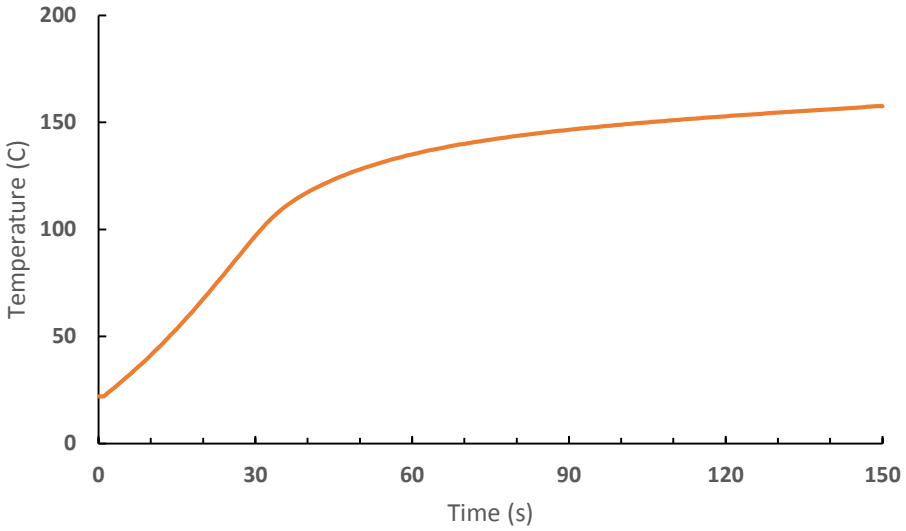

Figure 2-3: BRI results of 50 kW fire with fixed 0.6 m door width.

Figure 2-4 shows the BRI calculated hot gas layer depth over in a 50 kW fixed 0.6 m door width simulation. The smoke layer height appears to reach steady state shortly after the one minute mark and levels out at 1.03 m.

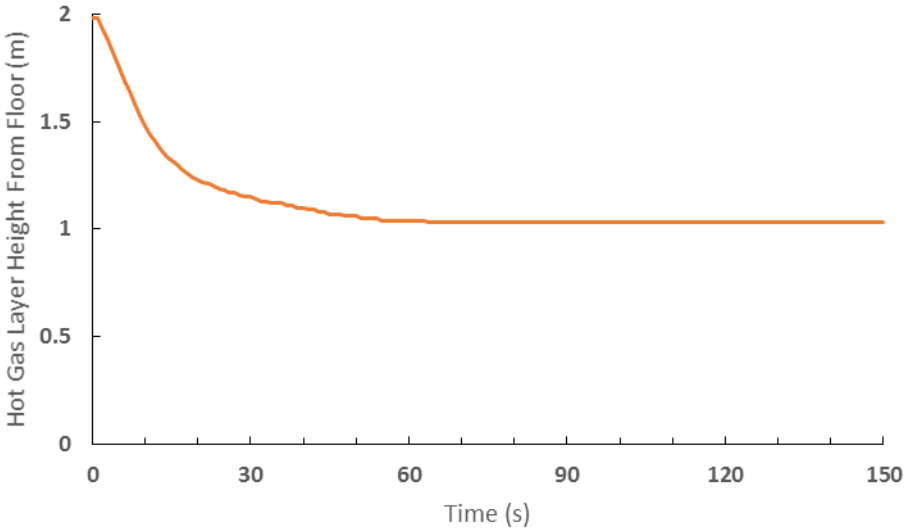

Figure 2-4: BRI hot gas layer depth vs measured hot gas layer depth. Solid line is BRI results, dotted line is experimental data.

2.2.3 Identifying Multiple Input Variable Parameters

To identify what input variables would appropriately reduce the solution space of the optimization problem, a series of exploratory BRI simulations were conducted. Initially, the hypothesized expectation was that using the temperature of the fire room (the default input in the established IFM) in conjunction with the temperature of the adjacent hall room would allow for a single door width and fire size that would yield such a measurement. The MQH correlation shows that fire room temperature is a function of door width. Thus, the hot gas layer temperature in any given BRI simulation must be sensitive to both the fire size, and the width of the door for the door size to be unique calculated.

Figure 2-5 shows BRI simulations with fire sizes of 10, 25, 50, 75, and 100 kW and the subsequent results on hot gas temperatures while the fire door width remained fixed at 0.6 m. For each additional 25 kW, the hot gas layer temperature goes up approximately 60 ºC. These results show hot gas layer temperature is directly affected by fire size.

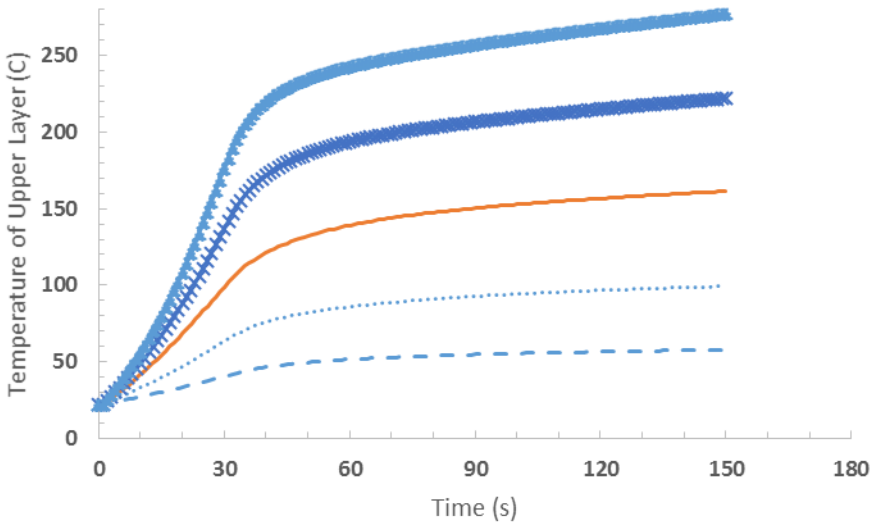

Figure 2-5: BRI data of varying fire sizes with fixed door widths on temperature in fire room. Door width was 0.6m. Dashed line is 10 kW, dotted is 25 kW, solid is 50 kW, X is 75 kW, triangles are 100 kW.

Figure 2-6 shows BRI simulations with fire door widths of 0.01, 0.1, 0.3, 0.6, and 1.2 m and the subsequent results on hot gas temperatures in the fire room while the fire size remained fixed at 50 kW. The MQH correlation predicts that the hot gas layer temperature will vary with the width of the fire door on the order of the width to the one third power. Thus if a door width is doubled, the change in temperature would be reduced by 20%; if the door width is reduced by half, then the temperature would increase by 25%. However, the MQH prediction is not seen in Figure 2-6. As door size is cut in half from 1.2 to 0.6 to 0.3, the increases are less than 7% and get smaller with each step. This result is likely due to the fact that the MQH correlation assumes a series of compartments or a compartment opening into ambient conditions. In the configuration used in the BRI simulations, the compartment is a nearly sealed, small three-room configuration.

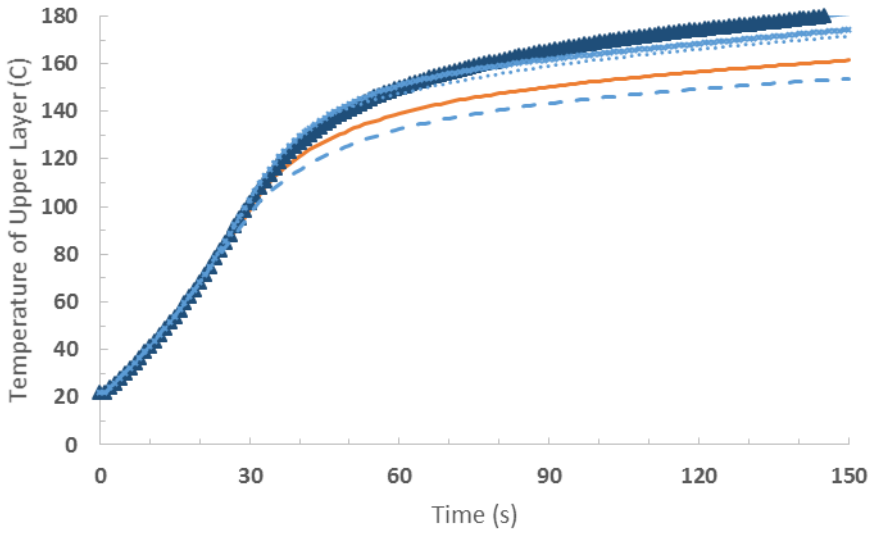

Figure 2-6: BRI data of fixed fire sizes varying fixed door widths on temperature in fire room. Fire size was 50 kW. Dashed line is door width of 1.2m, solid line 0.6m, dotted line 0.3m, X's 0.1m, triangles 0.01m.

Figure 2-7 shows BRI simulations with fire sizes of 10, 25, 50, 75, and 100 kW and the subsequent results on hot gas layer height in the fire room while the fire door width remained fixed at 0.6 m. For each additional 25 kW, the hot gas layer height development hardly changes at all. This result is counter to expectation, typically a larger fire would lead to a more rapid height development due to increase mass flow rate as described by the physics in section 2.2.1. This result could be due to the constrictions in air flow

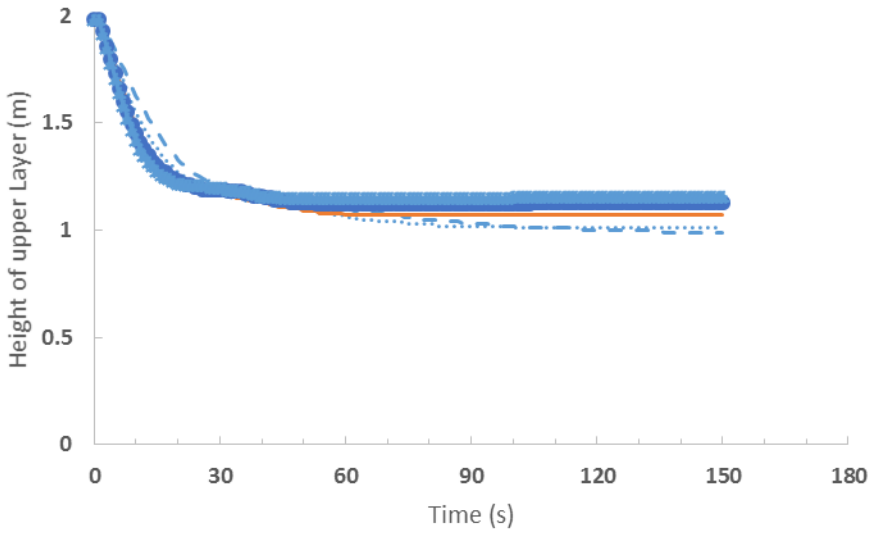

Figure 2-7: BRI data of varying fire sizes with fixed door widths on hot gas layer depth in fire room. Door width was 0.6m. Dashed line is 10 kW, dotted is 25 kW, solid is 50 kW, X is 75 kW, triangles are 100 kW.

Figure 2-8 shows BRI simulations with fire door widths of 0.01, 0.1, 0.3, 0.6, and 1.2 m and the subsequent results on hot gas layer height in the fire room while the fire size remained fixed at 50 kW. As door size is reduced, the hot gas layer in the fire room descended significantly lower, particularly from 0.3 m to 0.1 and 0.01 m. This result was expected, as a narrower door width lets out hot gases slower, leading to a greater build up in the fire room. In the configuration used in the BRI simulations, the compartment is a nearly sealed, small three-room configuration.

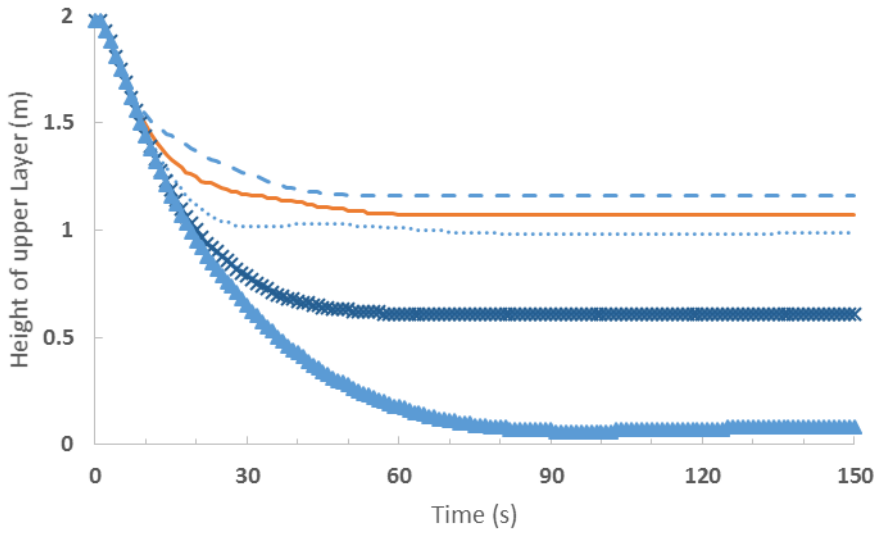

Figure 2-8: BRI data of fixed fire sizes with varying door widths on hot gas layer depth in fire room. Fire size was 50 kW. Dashed line is door width of 1.2m, solid line 0.6m, dotted line 0.3m, x's 0.1m, triangles 0.01m.

Physics that could explain unexpected phenomenon can be found in the Vent Flows in Section 2 of the SFPE Handbook 4th Ed [20]. With compartments in series, the flow across any given vent is described by the pressure across that vent. In a series of vents where steady state mass conservation can be assumed (and steady state results with regards to the hot gas layer depth appear at roughly 70 seconds into tests), the pressure across an arbitrary vent K can be described as:

$$\Delta p_k = \left(\frac{A_e}{A_K}\right)^2 \Delta p$$

Where Δp_k is the pressure across vent K, A_K is the area of vent K, Δp is the pressure across the entire series of compartments, and A_e is the equivalent area given by:

$$A_e = \left(\frac{1}{{A_1}^2} + \frac{1}{{A_2}^2} + \cdots + \frac{1}{{A_k}^2} + \cdots + \frac{1}{{A_N}^2}\right)^{-1/2}$$

Figure 2-1 illustrates the effective vent area in a series of compartments. These equations identify that if one vent in a series is very small proportionally to the other

vents, it reduces the pressure across any individual vent. Because the final vent in the three-room compartment scenario is a very thin vent of small area, it impacts the flow not only from Room 3 to the outside, but from Room 1 to 2 and 2 to 3. This phenomenon may lead to the results of door width not having the expected result on the fire room hot gas layer temperature because the difference in flow of the hot gas layer out of the fire room is limited by the final small vent in the series. These physics may also explain why the door width has a substantially larger impact on hot gas layer height as it approaches 0.1 m wide, the width of the final vent in the series. A calculation of the equivalent area impact, assuming 2 m tall doors that are 0.6 wide, three equal areas is shown in Table 2-1. Making a small final vent drops this figure significantly and subsequently that doubling the first door width has relatively little impact after the final door width is reduced.

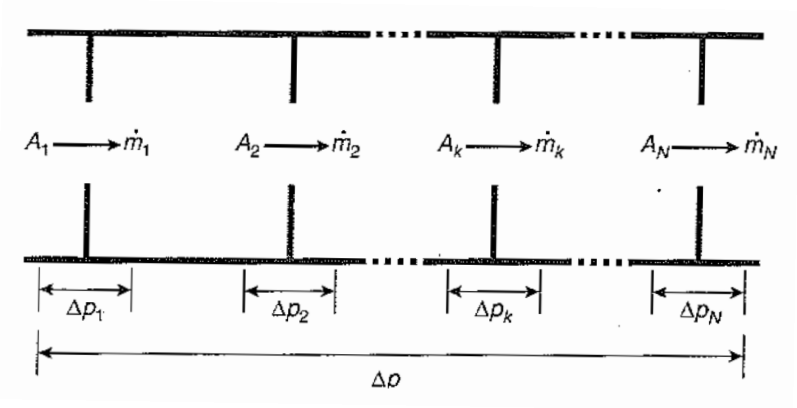

Figure 2-9: Effective vent area series of vents. [20]

Table 2-1: Equivalent area calculations demonstrating how a small final vent severely limits equivalent area. A1,A2,A3 represent areas of door widths from Room 1 to 2, 2 to 3, and 3 to ambient respectively. Units of m^2.

Scenario #	A1	A2	A3	A_e
1	1.2	1.2	1.2	0.693
2	1.2	1.2	0.2	0.195

3	2.4	1.2	0.2	0.197

Ultimately, hot gas layer temperature is strongly dependent on fire size, but weakly dependent on door width. Conversely, hot gas layer height is strongly dependent on door width, and weakly dependent on fire size. These results indicate that using neither two temperature signals nor two hot gas layer height signals for input may not be able to adequately identify a unique solution to both fire size and door width. Thus it was determined to one of each signal type, given their unique strong dependencies on fire size and door width, would identify a unique solution. Note that this approach may not be required in scenarios where compartments have a larger series of rooms (or larger rooms) or a compartment series that opens to ambient conditions. In such a case, temperature signals from adjacent rooms may be able to determine a unique solution; further exploration is needed on that topic.

2.2.4 Genetic Algorithm Approach

The inverse fire model was designed to calculate the heat release rate and fire door width that most closely produces a hot gas layer temperature and depth compared to the input temperature and depth. As mentioned in the literature review, an optimization tool is needed to calculate a best match. A genetic algorithm (GA) was used for this IFM due to its general robustness with multi-variable problems and its ability to avoid incorrectly settling on local minima or maxima.

A genetic algorithm is made of several components. First, there is an initial population. The “initial population,” in this case, is a series of BRI simulations with randomly assigned fire sizes and door widths. Each randomly generated BRI simulation will produce an output of a hot gas layer temperature and depth over the same period of

time as the laboratory experiments. This output temperature and depth will be compared to the input temperature and depth and be assigned a fitness value. The equation below shows the fitness function:

$$f = \left(\frac{\sum_{n=1}^{N} \left(\left(T_{BRI}(t_n) - T_{ref}(t_n) \right)^2 + C\left(D_{BRI}(t_n) - D_{ref}(t_n) \right)^2 \right)}{N} \right)^{-1}$$

where N is the total number of time steps, T_{BRI} is the temperature at a given time step, T_{ref} is the input temperature a given time step, D_{BRI} is the layer depth at a given time step, and D_{ref} is the input layer depth at a given time step. C is a constant set to be equal to 50 to raise the magnitude of the mean squared error of the layer depth to be on the same order as the temperature error. In this definition, the variance of the hot gas layer temperature and depth with respect to the input values is calculated such that less variance leads to a larger f and is a greater degree of fitness. Conversely, a smaller f means that there is greater variance between the input signal and a given individual in the population. A perfect fit, in this definition, would lead to infinite fitness and close fits would lead to large values. A fitness value of 1 would indicate an average temperature difference of 1 degree Celsius over the course of the simulation time. Each simulation in the initial population is compared to the input signal and prescribed the above fitness value.

Once the initial population of simulations is completed and a fitness value is calculated for each "individual" in the population, the most-fit simulation is identified. Based on that most fit simulation, a new "generation" of simulations is produced based off the properties of that simulation. As new simulations are "born" into this new

generation's population, various forms of crossovers and mutation functions are performed to explore a variety of different fire sizes and door width values to examine how changing these parameters affects the fitness value. A crossover is a process that takes two individual simulations to produce two new individuals with combined characteristics. A mutation takes an individual and changes one or more characteristics to produce a new individual. The GA employs several different crossover and mutation functions to each population based on the most-fit solution from that population. The number of mutations and crossovers performed is a prescribed figure within the GA that is independent of other variables. This number was very low, less than 10 for each mutation, irrespective of whether the population was 20 or 2000. For this research, the number of mutations and crossovers was changed to be based on a percentage of the initial population. Table 2-2 below shows the crossover and mutation rates as a percent of the initial population.

Table 2-2 Table of genetic algorithm mutation rates based on population size.

Crossover/Mutation Type	% of initial population
Boundary Mutation	6
Multi-nonuniform Mutation	16
Nonuniform Mutation	12
Uniform Mutatation	12
Point Mutation	12
Arith Crossover	8
Heuristic Crossover	8
Simple Crossover	2

Each new population produces is a "generation." As each generation is produced, a new population is formed and a new best-fit individual is identified to then calculate the

next generation. This process is iterative and based on a prescribed number of generations. The number of generations used in this work was arbitrarily prescribed based on convergence. After fifty generations, the next most-fit solution was the same as the first solution to roughly 0.01 kW. In future work, a formal convergence criteria could be prescribed, but in this proof of concept this arbitrary generation value was used.

The end result after a number of generations was a BRI simulation that had a fire size and door width that generated a hot gas layer temperature and depth most similar to the input value. That fire size and door width was the IFM's guess as to their true value. This guess was the final result of the IFM alongside a series of plots comparing these values.

Originally, MATLAB was used to invoke the GA and BRI iterations. In this study, GNU Octave, an open source language for numerical simulation that runs MATLAB code, was used in place of MATLAB for the convenience of running simulations from any computer [21].

2.2.5 Simulation Procedure

A series of inverse fire models was run. Six different types of tests were run. Tests #1-3 were synthetic single room tests while Tests #4-6 were the full three compartment tests based on experimental data. In Test #1-3, single room tests were run to examine the principal of the IFM in a basic environment. This artificial test was done as a check to see if the IFM behaves as expected in the simple case of a single room compartment opening to outside conditions. Because the IFM previously had not used two input signals to solve for two unknown variables, a baseline of performance was established before proceeding

to the more complex, multi-room case. Table 2-3 shows the test matrix for the IFM simulations. In tests where there was only one variable solved for by the IFM, that variable was fire size and subsequently the door width was assumed fixed at 0.6 m, the actual door width in the experiments. In tests where there was only one input signal, that input signal was hot gas layer temperature.

Table 2-3 Text matrix for IFM experiments. 1 variable tests only solve for fire size, 1 input signal tests use temperature.

Test #	# of Rooms	# of Variables	Input Signals	Test Abbr.
1	1	1	1	1R1V1S
2	1	2	1	1R2V1S
3	1	2	2	1R2V2S
4	3	1	1	3R1V1S
5	3	2	1	3R2V1S
6	3	2	2	3R2V2S

While there was no experimental data Test #1 starts with solving only for fire size and uses only temperature for input. Then in Test #2, the IFM solves for fire size and fire door width, but still only uses temperature for input. Finally Test #3 uses both temperature and depth for input to solve for fire size and fire door width. Test #1 serves as a baseline for Tests #2 and Test #3 because there is no experimental data for the single room case. However, Neviackas previously demonstrated the IFM was already capable of accurately identify fire size using only temperature signals from synthetic data [15]. As a result, the fire size results of Test #1 are the baseline for comparison for the fire size results of Test #2 and Test #3. The hot gas layer depth results from Test #1 were then the input for Test #3, where two input signals were used.

Tests #4-6 represented the full multi-room compartment fire scenario. In Test #4, the IFM solved for only fire size and used only temperature as the input. Test #5 repeats

Test #4 but assumed no knowledge of the door width (thus fire size and door width were the results). In Test #6, fire size and door width were solved for by using both the hot gas layer temperature and depth.

Tests #1 and #4 represent using the IFM as it had been used in previous work. There was one input signal, temperature, and one variable solved for, fire size. Test #2 and #5 increase the complexity by taking away the assumption of door knowledge and requiring the IFM to solve for that value in addition to fire size. These tests were designed to show some degree of failure due to the lack of unique solution for the IFM to settle on. With such failure established, Tests #3 and #6 were designed to use two input signals to solve for two variables and identify a unique solution to the multi-variable problem.

Each test was run with an initial population of 700 for 50 generations. In the initial population, the GA randomly generated fire sizes between 5 kW and 2500 kW and door widths between 0.1 m and 1.2 m. For comparison, the laboratory experimental conditions were a 50 kW fire with a 0.6 m door width.

2.2.6 Simulation Assumptions

Below is a list of assumptions used in both the one-room and three-room IFM simulation tests.

- Compartment geometry and layout were known
- Building materials were known
- Initial location of fire was known
- Ambient starting temperature of 22 degrees Celsius and 1 atm pressure, both inside and outside the configuration

2.2.7 Comments

This proof of concept was not total simulation time. Simulations were on the order of 20-60 minutes per complete test. The simulations were run on normal home desktop/laptop computers and were not optimized for speed. The IFM could be run much faster with technology and optimizations, however, as mentioned in the Literature Review, there are already faster tools such as the Ensemble Kalman filter for performing optimization problems.

Chapter 3: Results and Analysis

Detailed thermocouple data was measured from a medium scale, multi-room compartment fire to provide input to a series of inverse fire model simulations to test for uniqueness of solution and accuracy. The following section presents and discusses the results of the compartment fire experiments and inverse model simulations. The first consideration of each result was the uniqueness of the solution; when run multiple times, does the inverse fire model (IFM) produce the same result each time? The second consideration, accuracy, was considered by comparing the input experimental data to the resulting temperature and hot gas layer signals. Additionally, the accuracy is considered in terms of the calculated unknowns of fire size and fire door width compared to the experimental values.

3.1 Compartment Fire Experiment Results

The raw temperature data from experiments was not in a useful form for inverse fire modeling as the zone fire model relies on an average hot gas layer temperature instead of spatial temperature measurements. Using the process outlined in section 2.2.1, an average hot gas layer temperature is obtained from the raw data. Figure 3-1 below shows the average hot gas layer temperature over time, starting from the time the burner is ignited.

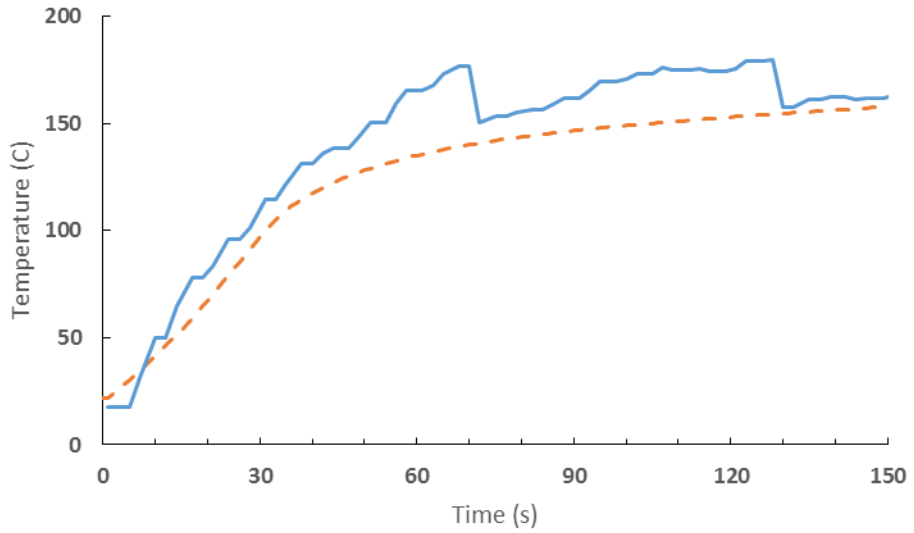

Figure 3-1: Input temperature signal (solid line) compared to BRI simulation temperature results (dashed line) of 50 kW fire.

The input hot gas layer temperature is consistently hotter than the BRI simulation of the same fire size. This error is either due to a combination of the sensor measurements and the approximation for the hot gas layer temperature, inaccuracies in the BRI model, or some combination of both. As a result of this discrepancy, it is expected that the IFM would over predict the HRR due to the fact that BRI would need a greater than 50 kW fire size in order to match temperature signals.

Figure 3-2 below shows a comparison of the input hot gas layer height from experimental measurements and the BRI prediction of the hot gas layer descent of a 50 kW fire. The hot gas layer height from experiments experiences a more gradual decline over time than the BRI prediction of a 50 kW fire. This error is either due to a combination of the sensor measurements and the approximation for the hot gas layer height, inaccuracies in the BRI model, or some combination of both. This discrepancy could lead to the IFM over predicting how open the door is towards the beginning of the

simulation and too closed towards the end as it finds a BRI simulation that best matches the input signal.

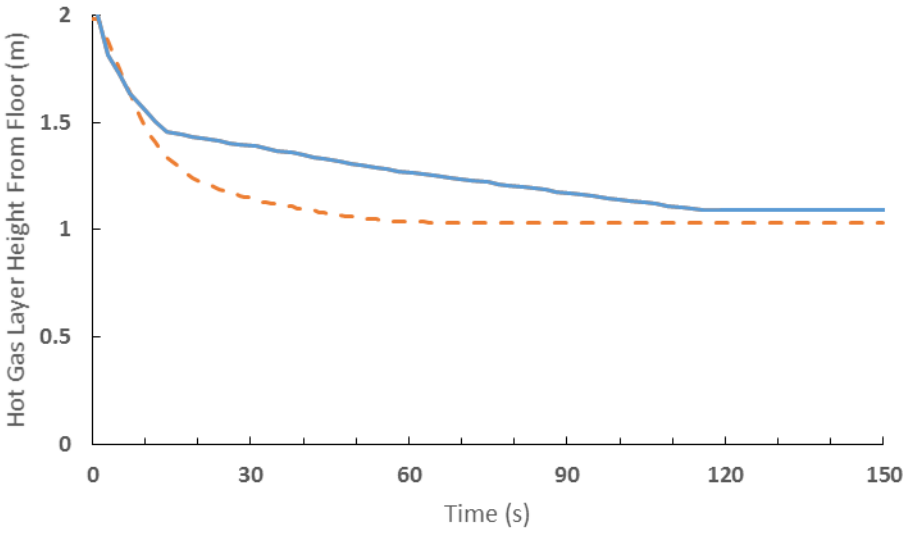

Figure 3-2: Input hot gas layer height signal (solid line) compared to BRI simulation hot gas layer height results (dashed line) of 50 kW fire.

3.2 Inverse Fire Model Results

The IFM results are presented in summarized form. Each of the 6 different tests were run 30-50 times. Representative plots from these tests will be shown in the following section. For the results of each tests, refer to Appendix B.

3.2.1 Test #1 One Room, One Variable, One Input Signal (1R1V1S) Results

The 1R1V1S test used the same temperature input signal as obtained from the three room compartment fire. The one unknown variable being calculated is the HRR. Door width was a constant 0.6 m for this test.

The results of this test appear unique. Multiple runs of the IFM yielded only identical results.

Figure 3-3 below shows the temperature results of this test compared to the experimental results. The temperature results match well with input data with a mean squared error (the inverse of the fitness value) of 6.4 degrees Celsius.

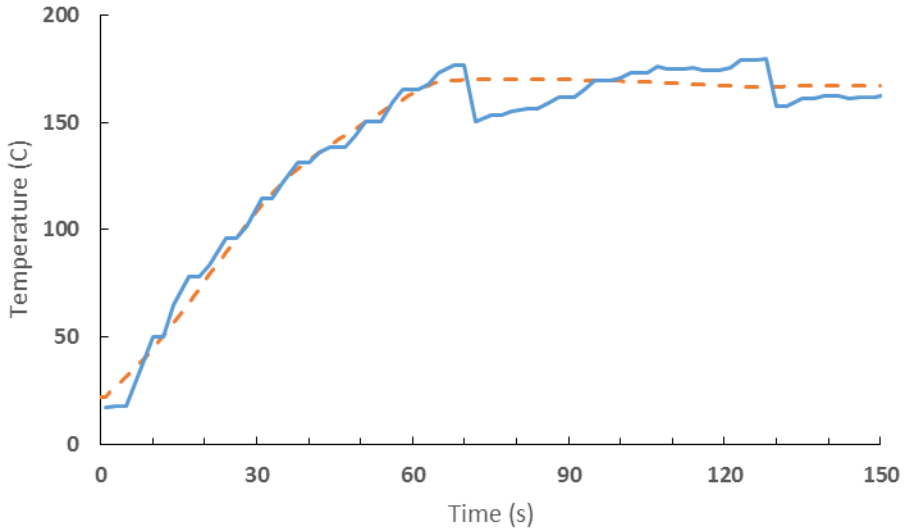

Figure 3-3: Temperature results of 1R1V1S test (dashed line) compared to experimental result (solid line).

Figure 3-4 below shows the HRR results of this test compared to the experimental results. The HRR results differ significantly from experimental results, reaching nearly twice the HRR. Given that the experimental results are from a multi-room compartment with no vent to ambient conditions, and this test is of a single room with a full door way to ambient conditions, the discrepancy is expected. The HRR results. The consistent overprediction of the fire size was expected due to the increased requirement for fire size to produce enough heat in a single room environment where the fire door leads to ambient conditions instead of further compartments in addition to the expectation that the IFM would over predict compared to the baseline BRI test of a 50 kW fire producing lower temperatures than obtained in experimental data.

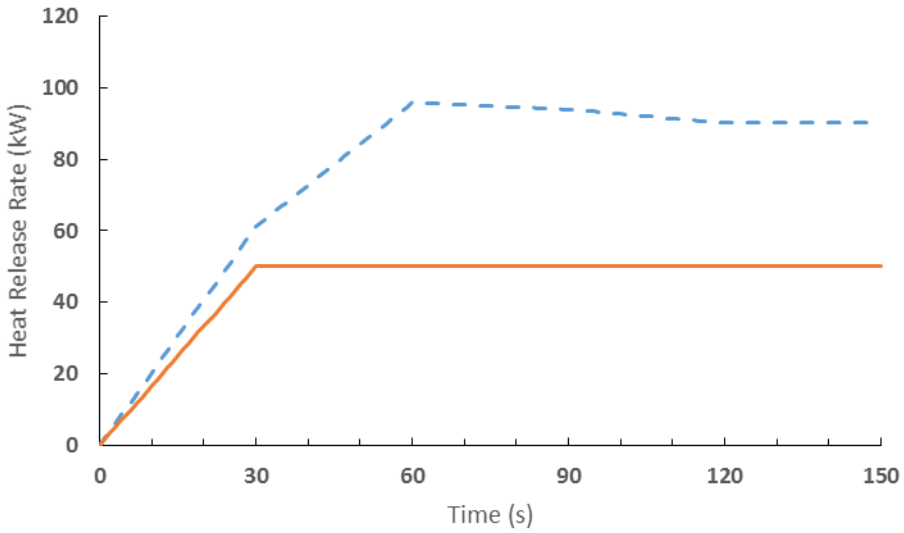

Figure 3-4: HRR results of 1R1V1S test (dashed line) compared to experimental result (solid line).

The above results represented a unique solution identified by the IFM. Below, Figure 3-5 shows the hot gas layer height result from this test. This hot gas layer height signal had Gaussian noise added for use as the input hot gas layer height signal for Test #3.

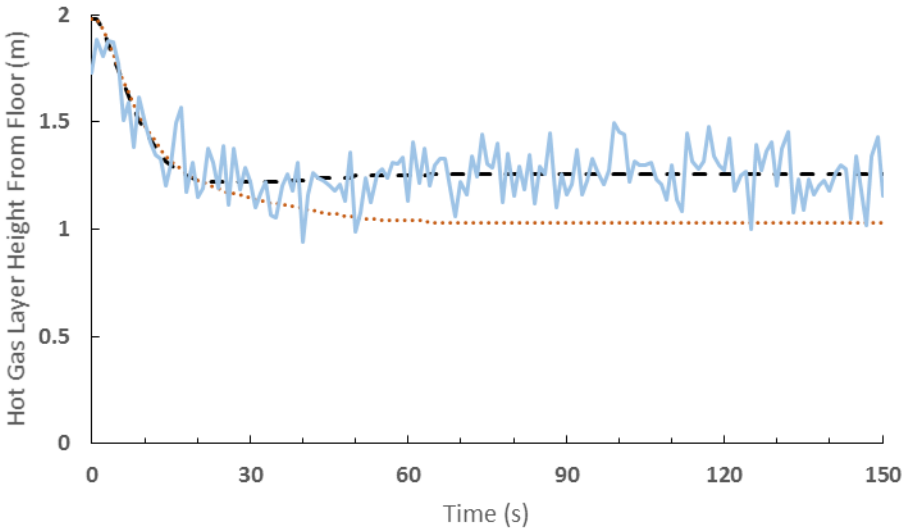

Figure 3-5 Hot gas layer depth results from IFM (dashed line) compared to BRI baseline (dotted line). A new input signal for Test #3 is produced by adding noise to the IFM calculation (solid line).

3.2.2 Test #2 One Room, Two Variable, One Input Signal (1R2V1S) Results

The 1R2V1S test used the same temperature input signal as obtained from the three room compartment. The two unknown variables being calculated are the HRR and the door width.

The results of this test were not unique. Multiple runs of the IFM yielded many different results.

Figure 3-6 below shows the temperature results of this test compared to the experimental results. The temperature results matched well with input data with a mean squared error of 4.18 degrees Celsius. Between consecutive runs of the IFM, temperature signals tended to follow this approximate form +/-5%.

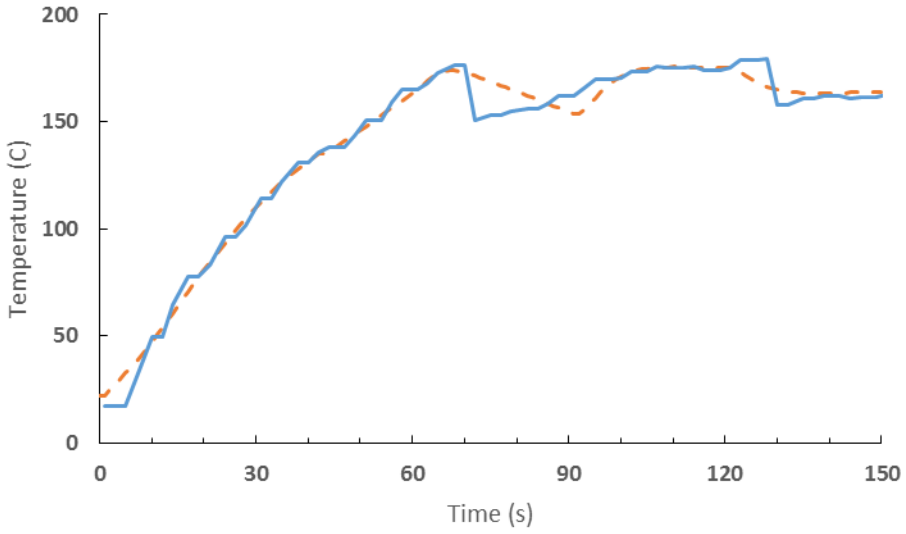

Figure 3-6: Temperature results of 1R2V1S test (dashed line) compared to input result (solid line).

Figure 3-7 below shows a sample of three HRR results of this test compared to the experimental results. The HRR results were not unique and there were a variety of

solutions determined by the IFM. Some results varied by as much as 50% (~130 kW vs ~80 kW) and were very inconsistent. The multiple results were expected due to the lack of unique solution to the multivariable problem with only one input signal, discrepancies in input data and BRI baseline for a 50 kW fire size discussed in section 3.1, and the increased requirement for fire size to produce enough heat in a single room environment where the fire door leads to ambient conditions instead of further compartments.

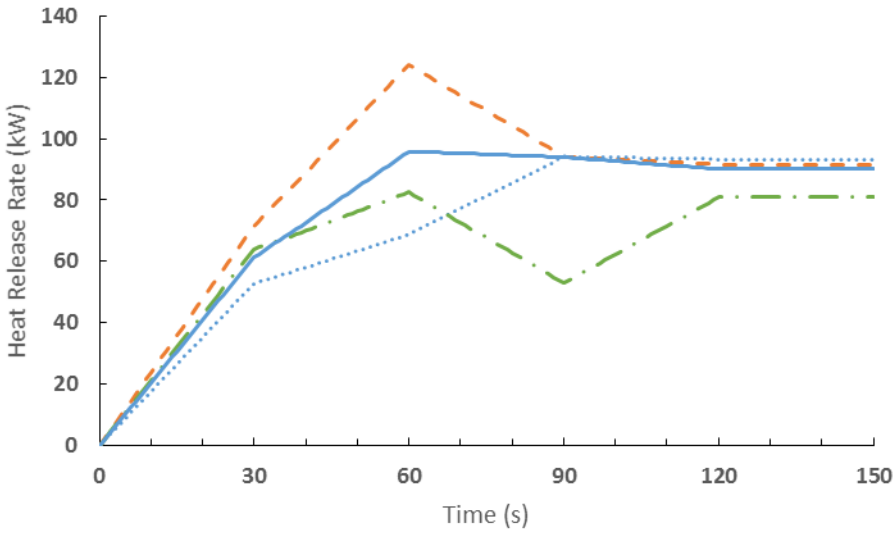

Figure 3-7: Three HRR results of 1R2V1S tests (dashed, dotted, and dash-dot lines) that present a lack of unique solution paired with the solution from Test #1 (solid line).

Figure 3-8 below shows a sample of three door width results of this test compared to the experimental results. The door width results were not unique and there were a variety of solutions determined by the IFM. The door width results appear almost random, due to the likely large number of possible combination of fire size and door width in the single room scenario that can produce the same temperature curve.

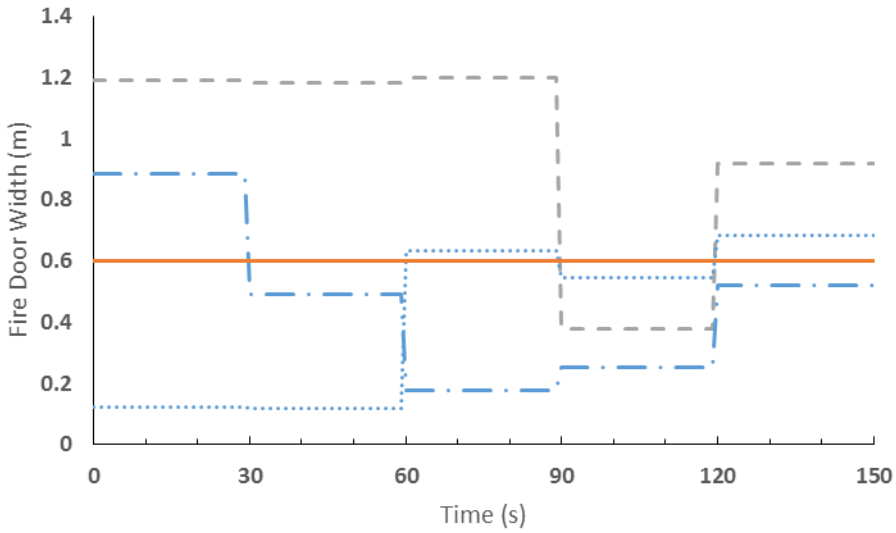

Figure 3-8: Three door results of 1R2V1S tests that present a lack of unique solution (dashed, dotted, and dash-dot lines) compared to the actual door width (solid line).

3.2.3 Test #3 One Room, Two Variable, Two Input Signal (1R2V2S) Results

The 1R2V2S test used the same temperature input signal as obtained from the three room compartment fire but used the hot gas layer height from the results of Test #1. The two unknown variables being calculated are the HRR and the door width.

Figure 3-9 below shows the temperature results of this test compared to the experimental results. The temperature results match well with experimental data with a mean squared error of 7.3.

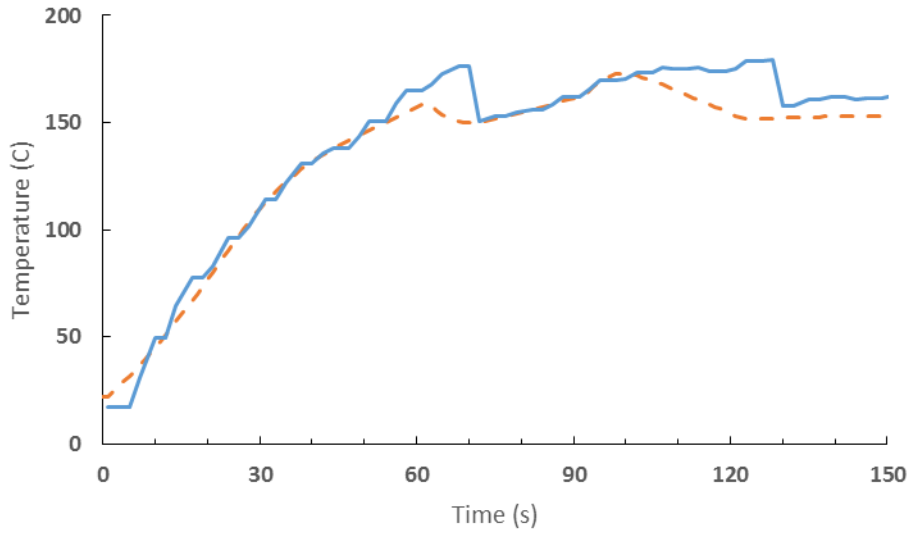

Figure 3-9: Temperature results of 1R2V2S test (dashed line) compared to input result (solid line).

Figure 3-10 below shows the HRR results of this test compared to the results of Test #1. The Test #1 results are the closest form of "correct" answer to serve as a baseline for comparison. The HRR results were unique and match well within 20% of the fire size obtained from Test #1. The consistent prediction of the fire size was expected due to the result being unique and one of the input signals being obtained from a BRI simulation result of the first input temperature. Because BRI used the input temperature to generate the smoke layer height, it is expected the IFM could replicate this scenario very precisely compared to only experimental input data that will be used in Tests #4-6.

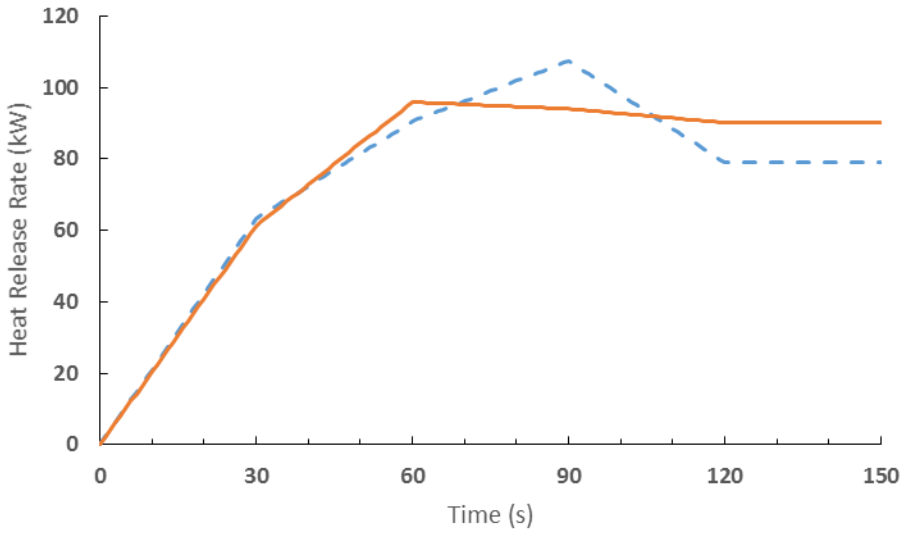

Figure 3-10: The HRR results of 1R2V2S tests that present a unique solution (dashed line) compared to the HRR obtained from Test #1 (solid line).

Figure 3-11 below shows the door width results of this test compared to the experimental results. The door width results were unique. The door width results were all within 15% of the experimental door width except from 60-90 seconds where the door width jumps to 0.91 m (50% greater than fixed width). This one time frame discrepancy may be due to matching the smoke layer signal more closely.

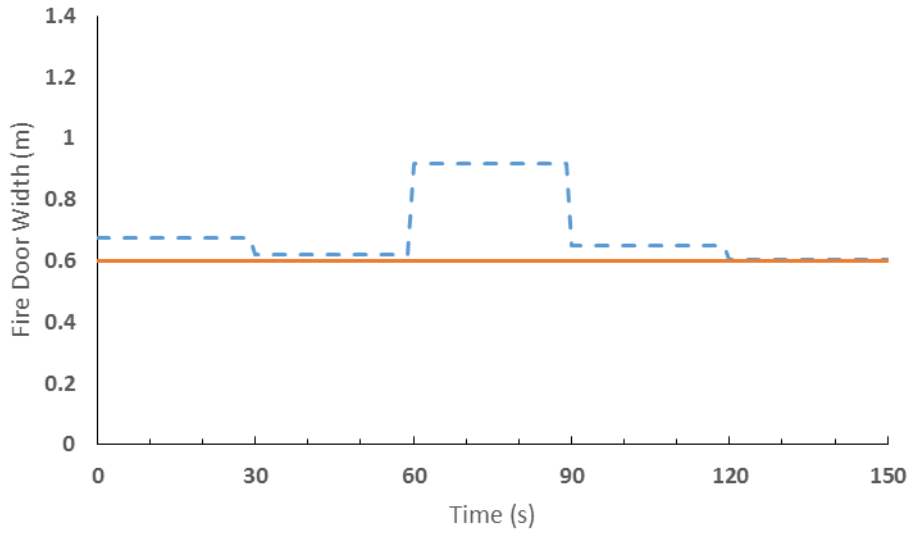

Figure 3-11: Door results of 1R2V2S tests (dashed) that present the unique IFM solution compared to actual door widths (solid).

Figure 3-12 below shows the hot gas layer height results from the 1R2V2S tests. The hot gas layer heights match very well with a mean squared error of 0.15 m. The accuracy in the 60-90 second time frame may have led to the abnormal door width result as the predicted HRR in this time frame is also higher than the expected HRR. The high accuracy of this result is expected due to the input data being provided by BRI itself from the results of Test #1. In the event of experimental data, such close matching would not be expected.

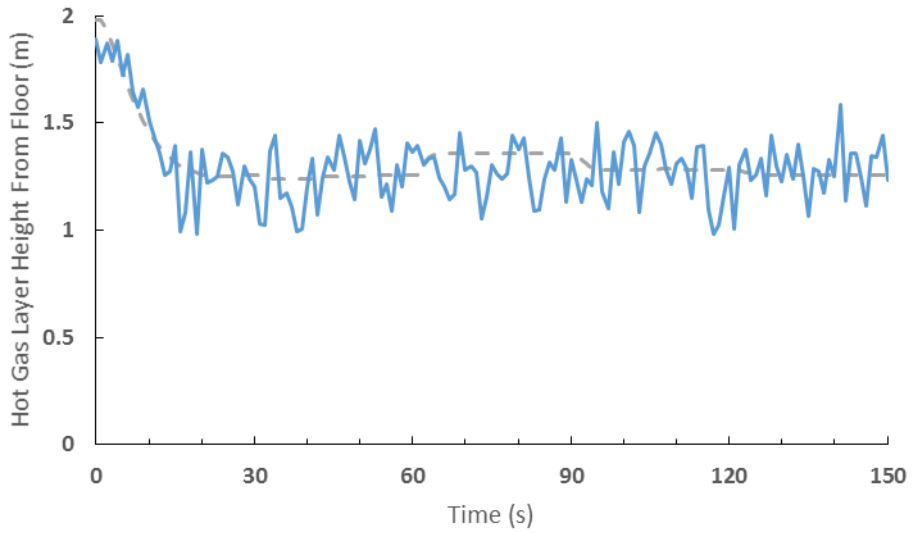

Figure 3-12: Hot gas layer height results of 1R2V2S test that present a unique solution (dashed line) compared to input noise signal (solid line).

3.2.4 Test #4 Three Room, One Variable, One Input Signal (3R1V1S) Results

The one unknown variable being calculated is the HRR. Door width was a constant 0.6 m for this test.

The results of this test appear unique. Multiple runs of the IFM yielded only identical results.

Figure 3-13 below shows the temperature results of this test compared to the experimental results. The temperature results match well with experimental data with a mean squared error of 6.7 degrees Celsius. The resulting temperature is higher than the BRI baseline curve for a 50 kW fire, so the HRR is expected to be overpredicted.

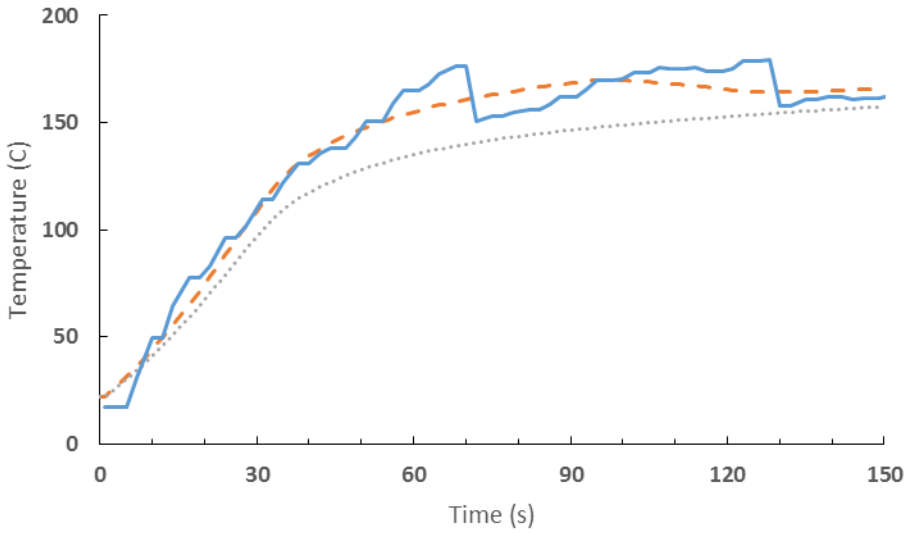

Figure 3-13: Temperature results of 3R1V1S test (dashed line) compared to experimental result (solid line) and the BRI baseline (dotted line).

Figure 3-14 below shows the HRR results of this test compared to the experimental results. The HRR results match well with experimental data with, within 20% of the experimental fire size. The consistent overprediction of the fire size was expected due to the discrepancies in input data and BRI baseline for a 50 kW fire size discussed in section 3.1.

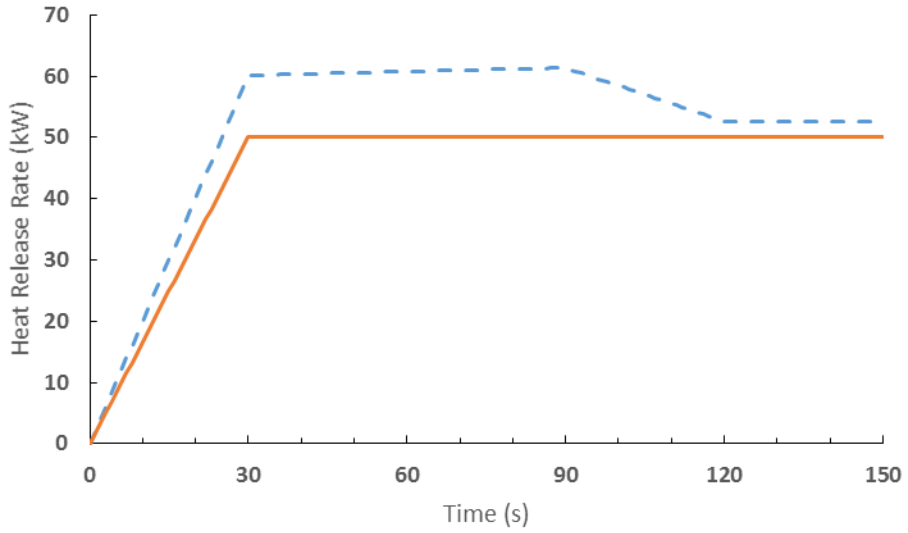

Figure 3-14: HRR results of 3R1V1S test (dashed line) compared to experimental values (solid line).

3.2.5 Test #5 Three Room, Two Variable, One Input Signal (3R2V1S) Results

The two unknown variables being calculated are the HRR and the door width.

The results of this test were not unique. Multiple runs of the IFM yielded many different results.

Figure 3-15 below shows the temperature results of this test compared to the experimental results. The temperature results match well with experimental data with a mean square error of 4.4 degrees Celsius.

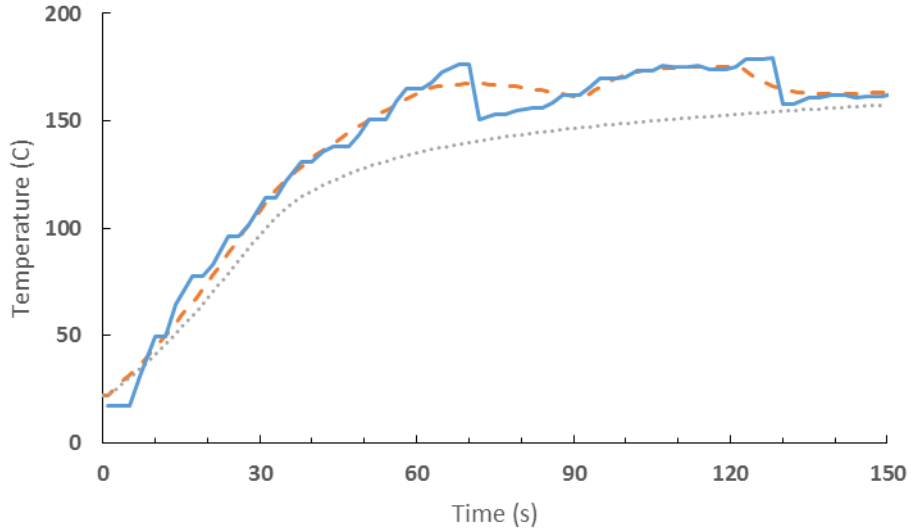

Figure 3-15: Temperature results of 3R2V1S test (dashed line) compared to experimental result (solid line) and the BRI baseline (dotted line).

Figure 3-16 below shows a sample of three HRR results of this test compared to the experimental results. The HRR results were not unique and there were a variety of solutions determined by the IFM. Values varied as much as 40% of the experimental HRR. The consistent overprediction of the fire size was expected due to the

discrepancies in input data and BRI baseline for a 50 kW fire size discussed in section 3.1.

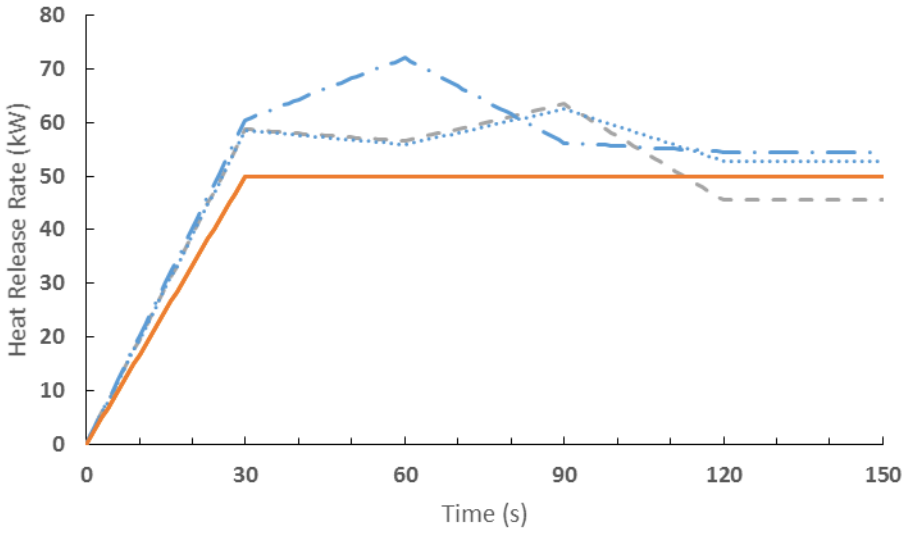

Figure 3-16: Three HRR results of 3R2V1S tests that present a lack of unique solution (dashed, dotted, and dash-dot lines) and the experimental value for HRR (solid line).

Figure 3-17 below shows a sample of four door width results of this test compared to the experimental results. The door width results were not unique and there were a variety of solutions determined by the IFM. The door width results appear almost random, due to the likely large number of possible combinations of fire size and door width that can produce the same temperature curve.

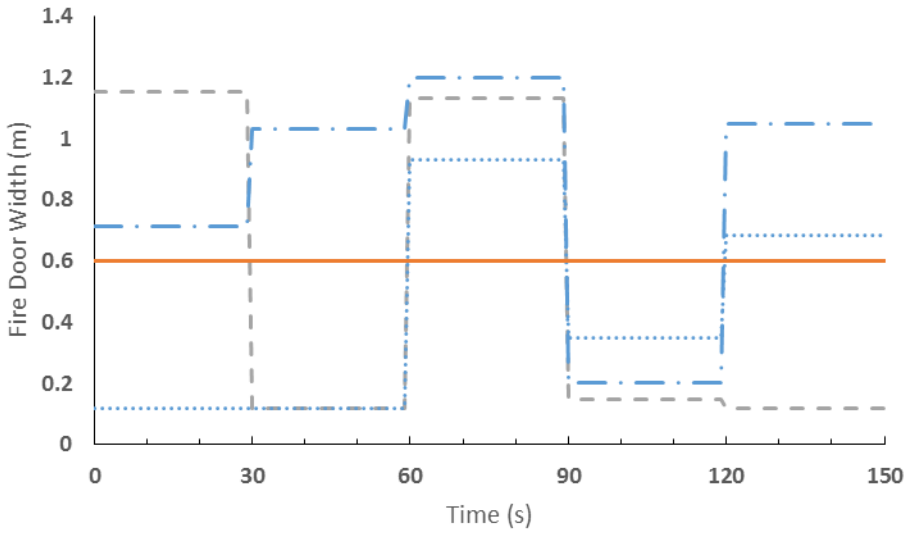

Figure 3-17: Three door results of 3R2V1S tests that present a lack of unique solution (dashed, dotted, and dash-dot lines) compared to experimental door width (solid line).

3.2.6 Test #6 Three Room, Two Variable, Two Input Signal (3R2V2S) Results

The 3R2V2S test used the same temperature input signal as obtained from the three room compartment fire but used the hot gas layer height from the results of Test #1. The two unknown variables being calculated are the HRR and the door width.

The results of this test appear unique. Multiple runs of the IFM yielded only identical results.

Figure 3-18 below shows the temperature results of this test compared to the experimental results. The temperature results match well with experimental data with a mean squared error of 4.78 degrees Celsius. The resulting temperature signal is greater than the BRI baseline for a 50 kW fire, so the HRR is expected to be overpredicted.

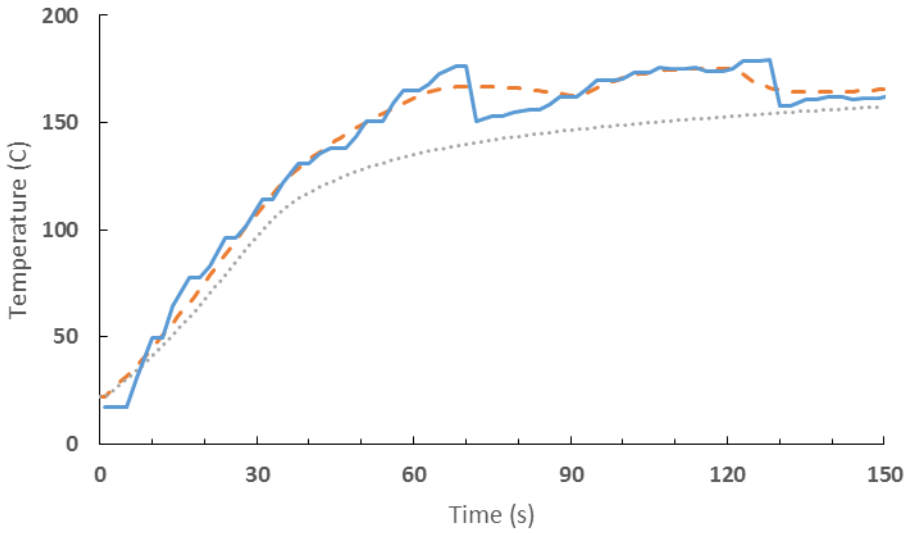

Figure 3-18: Temperature results of 3R2V2S test (dashed line) compared to experimental input (solid line) and BRI baseline (dotted line).

Figure 3-19 below shows the HRR results of this test compared to the experimental results. The HRR results were unique and match well within 40% of the experimental fire size. The consistent overprediction of the fire size was expected due to the discrepancies in input data and BRI baseline for a 50 kW fire size discussed in section 3.1.

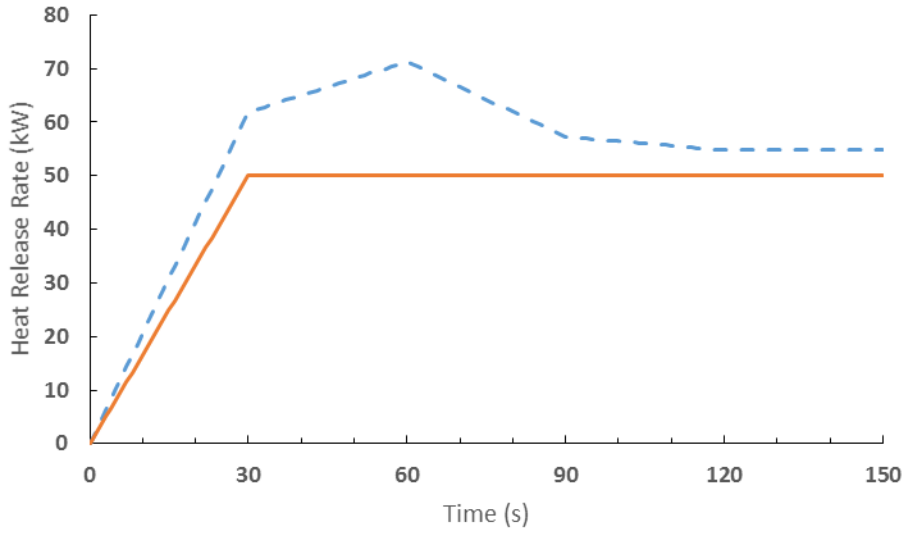

Figure 3-19: HRR results of 3R2V2S tests that present a unique solution (dashed line) versus experimental values of HRR (solid line).

Figure 3-20 shows the hot gas layer height results from the 3R2V2S tests. The hot gas layer heights match very well with the input data with mean squared error of 0.09 meters. The data does not match well with the BRI expectation of smoke layer height. By accurately representing the experimental smoke layer height, the door width result is greatly affected.

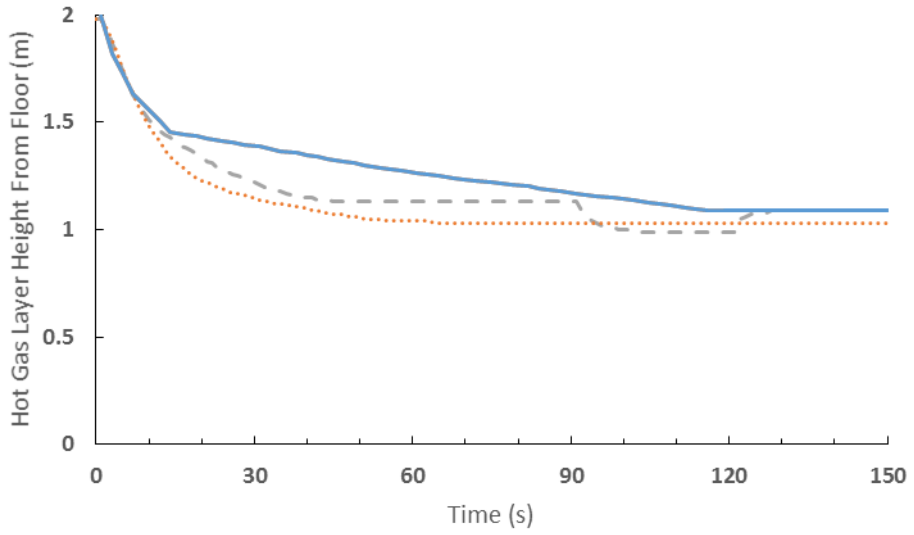

Figure 3-20: Hot gas layer height results of 3R2V2S test that present a unique solution (dashed line) with input hot gas layer height (solid line) and BRI baseline of a 50 kW fire (dotted line).

Figure 3-21 below shows the door width results of this test compared to the experimental results. The door width results were unique. The door width results show a more extreme case of the expected result. Based on the input hot gas layer signal and its discrepancy with the BRI prediction of the hot gas layer signal discussed in section 3.1, the predicted results be a somewhat wider opening than 0.6 m towards the beginning of the scenario and a somewhat more closed than 0.6 m width towards the end. The actual

results show a 1.2 m wide door (the maximum range in the IFM) for the first third of the scenario, with the door clamping down to 0.4 m wide then 0.9 m for the remainder. The dependency of the hot gas layer height on door width AND fire height is significant enough to make this result sensitive to input data.

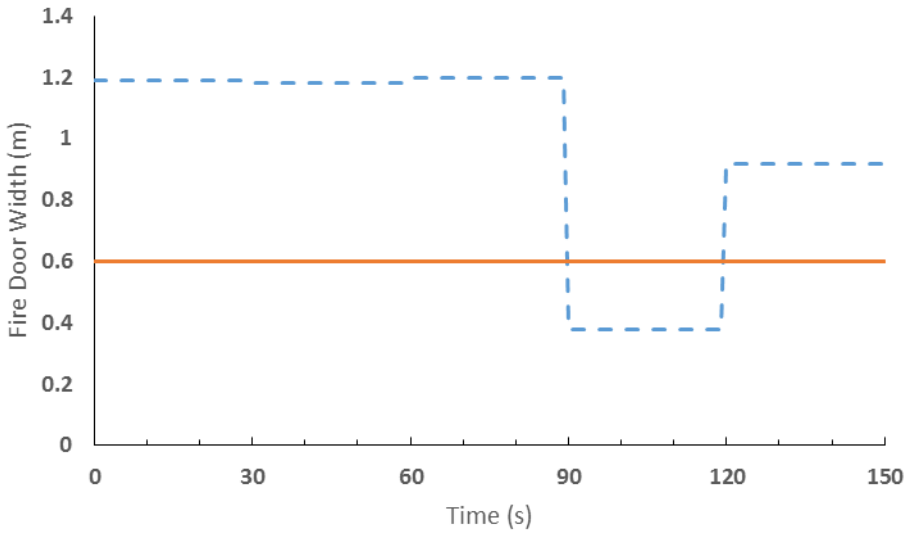

Figure 3-21: Door results of 3R2V2S tests (dashed) compared to actual door widths (solid) that present the unique IFM solution.

3.2.7 Summary of IFM results

The IFM results at first follow expectations but then have larger disagreements compared to the experimental scenario. In the simple one room case, there is first a unique solution with one input signal and one unknown variable (Test#1), followed by a non-unique solution when there are two unknown variables with no additional input signals (Test #2), and finally a unique solution once again with the addition of a second input signal (Test #3). It was expected the three room case would follow this pattern and the results show this expectation was correct.

However, the actual results overpredict on fire size and door width in the two unknown, two input signal tests (Test #6). The overprediction of fire size was expected across all results due to the discrepancy of the input temperature data and what BRI anticipates is the actual temperature of a hot gas layer created by a 50 kW fire. It is possible that either with better measurements, a different approximation technique, or a different threshold for hot gas layer temperature could provide more precise results. The door width has the largest discrepancy. Though the door width was fixed at 0.6 m, the IFM tended to overpredict it to 1.2 m, the maximum value in the prescribed range of door width exploration. While this result is unique, compared to the otherwise random results of Test #5, the result is not correct. This result is particularly sensitive to input data, and the input data used may not be accurate or the model may not be representative. In most cases of BRI runs, the descent of the hot gas layer is much faster than the experimental data indicated. This result is, in part, due to the fact that BRI has no transport lag, that is, hot gases generated by the fire instantly become a part of the hot gas layer and that layer is evenly distributed across the entire ceiling of the compartment. Ultimately the IFM calculates a unique solution when two variables are unknown. That success can serve as the baseline for future IFM development with more sophisticated measurements.

Chapter 4: Conclusion

A multi-room compartment fire experiment was performed to analyze the capability of an inverse fire model (IFM) to calculate the size of the fire and width of the door opening to the fire room used in the experiment based on temperature measurements from the compartment. Hot gas layer temperature and height measurements from a thermocouple were obtained using a thermocouple tree (a vertical array of temperature sensors) and these time based signals were used as input to an inverse fire model. The IFM then calculated what combination of fire size and door width could most closely reproduce the input temperature and height signals. The IFM used a genetic algorithm optimization tool in combination with the zone model BRI to run a barrage of simulations to compare to the input signals. These IFM tests represented the novel use of multiple input signals to solve a multiple variable problem where fire size and fire door width were assumed to be unknown. Previously, using only one temperature input signal led to a non-unique solution, where there were several "correct" pairs for fire sizes and door openings that could produce a given temperature.

The IFM was tested using one and two input signals to solve for two variables. In the case of one input signal, the IFM calculated a different solution almost every test. In the case of two input signals, the IFM calculated the same solution every time, demonstrating that multiple input signals can provide a unique solution to a multi-unknown problem. The inverse fire model produced a unique solution whenever two input signals were used.

The IFM was able to calculate the heat release rate of the fires to within 40% of their experimental values, typically coming within 10-20%, though all values were overpredicted. The discrepancies between the calculated values and the actual size of the experimental fire are primarily due to the difference between the input experimental temperature signal and what the zone fire model BRI expects the temperature results from the experimental fire size to be; i.e., the experimental results were from a 50 kW fire, but BRI anticipates a 50 kW fire to produce lower temperature than were provided from measurements. This discrepancy could be due to error in the BRI model, error in the measurements performed in the experiments, or over-approximations in the averaging technique used to calculate the average hot gas layer temperature from the thermocouple tree measurements. While the door width results were unique, they were incorrect, ranging from an overprediction of 100% to an underprediction of 30% over the course of the experiment. This result appears to stem from a sensitivity to the accuracy of the hot gas layer input data. The input signal used descended notably slower than the zone fire model BRI expected, causing BRI to predict a more open door width, whereas a closed door width would cause a faster descent. Because the result is unique, a more accurate input signal could lead to more accurate results.

Further research could assist in improving the results of the IFM. More experiments are necessary to test the robustness of the IFM with respect to physical data. More precise measurements of hot gas layer temperatures and depths could provide better input signals for use in conjunction with the IFM. Error introduced by the zone model BRI could be better understood and consequently characterized when compared to more accurate experimental data, allowing for a more accurate IFM result. Additionally, more

methods of multi-input signal approaches could be explored with better experimental data. The use of temperature inputs from measurements of adjacent rooms could also prove useful for compartments in series, and could help solve higher unknown problems. Further research could implement this IFM tool with a more modern and computationally efficient optimization tool that would allow more rapid computations. Research to make this IFM move from proof-of-concept into a potential product used in real applications would include researching using building sensors for producing measurement approximations of hot gas layer temperatures, utilizing that real-time temperature signal in the IFM as data is available, similar to Leblanc's work, and identifying ways of representing various fire sizes in meaningful ways to emergency first responders. A variety of studies are needed to make calculation of real emergency fires in buildings in real-time with high accuracy.

Appendix A Raw Temperature Data

The raw temperature measurements from the thermocouple tree at all ten heights can be seen below in Figure 4-1. The burned was ignited and the experiment began at roughly t=60 seconds.

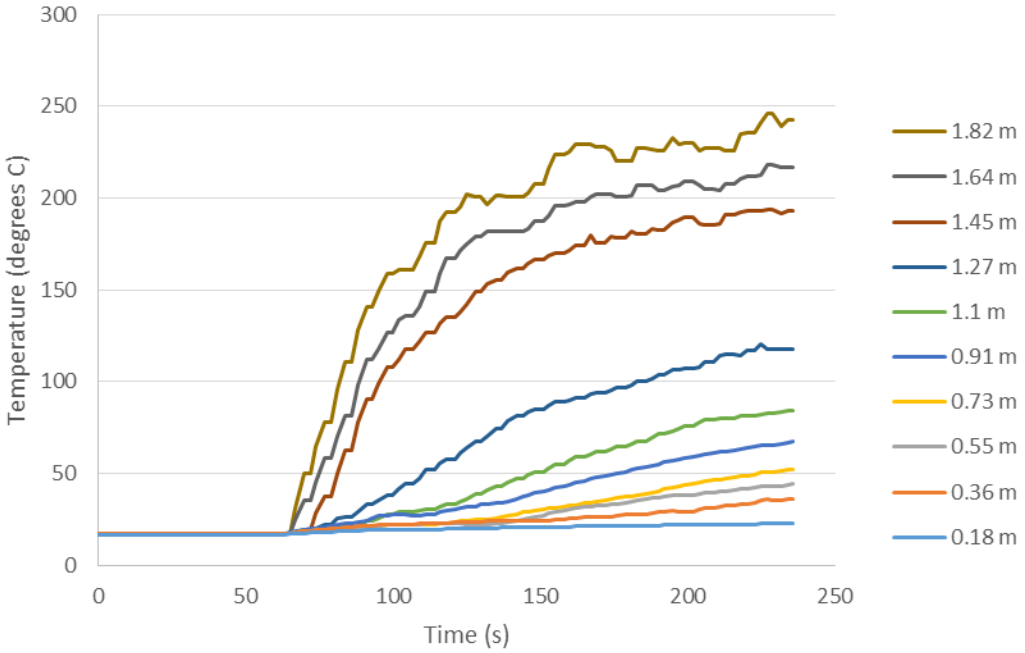

Figure 4-1: Raw temperature measurements from thermocouple tree. The hottest measurement is recorded at 1.82 m, the coldest at 0.18 m, each temperature measurement has approximately 18 cm spacing. The temperature measurements are labeled from highest to lowest, spatially.

Appendix B IFM Results

Test #1 Results

Table 4-1: HRR results from Test #1.

Run #	HRR at t=0s (kW)	HRR at t=30s (kW)	HRR at t=60s (kW)	HRR at t=90s (kW)	HRR at t=120s (kW)
1	0.00	61.28	95.85	94.02	90.13
2	0.00	61.24	95.89	94.02	90.13
3	0.00	61.24	95.88	94.01	90.13
4	0.00	61.20	95.91	94.01	90.14
5	0.00	61.23	95.87	94.00	90.14
6	0.00	61.24	95.81	94.03	90.15
7	0.00	61.24	95.88	94.02	90.13
8	0.00	61.25	95.86	94.00	90.12
9	0.00	61.24	95.82	94.01	90.13
10	0.00	61.24	95.88	94.01	90.13
11	0.00	61.24	95.90	94.01	90.14
12	0.00	61.20	95.89	94.02	90.13
13	0.00	61.24	95.82	94.02	90.13
14	0.00	61.24	95.88	94.01	90.13
15	0.00	61.24	95.83	94.03	90.14
16	0.00	61.20	95.91	94.02	90.13
17	0.00	61.24	95.80	94.02	90.13
18	0.00	61.23	95.89	94.02	90.13
19	0.00	61.24	95.82	94.02	90.13
20	0.00	61.20	95.88	94.01	90.13
21	0.00	61.27	95.86	94.03	90.14
22	0.00	61.24	95.87	94.01	90.14
23	0.00	61.24	95.80	94.02	90.13
24	0.00	61.21	95.91	94.02	90.13
25	0.00	61.23	95.84	94.03	90.15
26	0.00	61.23	95.84	94.01	90.14
27	0.00	61.26	95.76	94.02	90.13
28	0.00	61.26	95.76	94.02	90.13
29	0.00	61.24	95.83	94.04	90.14
30	0.00	61.24	95.88	94.02	90.13
AVG	0.00	61.24	95.85	94.02	90.13
STD	0.00	0.02	0.04	0.01	0.01

Test #2 Results

Table 4-2: HRR Results for Test #2.

Run #	HRR at t=0s (kW)	HRR at t=30s (kW)	HRR at t=60s (kW)	HRR at t=90s (kW)	HRR at t=120s (kW)
1	0.00	65.21	74.84	75.60	82.36
2	0.00	71.50	124.21	94.16	91.67
3	0.00	58.65	85.59	97.96	108.96
4	0.00	66.18	104.14	96.02	103.11
5	0.00	63.11	82.38	50.75	90.03
6	0.00	55.72	52.26	59.48	82.88
7	0.00	67.28	92.47	96.98	98.38
8	0.00	65.99	45.71	61.85	90.43
9	0.00	64.11	63.93	57.03	90.78
10	0.00	56.96	63.82	87.14	90.53
11	0.00	65.64	102.97	91.72	90.52
12	0.00	60.57	52.75	60.36	88.80
13	0.00	62.58	102.70	88.95	84.46
14	0.00	63.91	82.57	52.90	80.94
15	0.00	63.61	56.27	57.63	100.86
16	0.00	60.18	89.37	95.20	92.51
17	0.00	59.97	72.93	83.99	79.06
18	0.00	61.20	65.13	56.26	79.97
19	0.00	61.57	60.33	78.73	89.77
20	0.00	69.07	109.30	90.51	92.31
21	0.00	68.58	106.25	91.41	94.25
22	0.00	59.61	65.31	67.51	88.13
23	0.00	66.18	100.17	101.55	105.19
24	0.00	64.74	46.40	61.31	90.83
25	0.00	68.58	114.59	102.95	103.65
26	0.00	60.13	51.22	60.85	89.11
27	0.00	67.03	105.17	86.47	83.24
28	0.00	61.85	80.68	84.03	87.48
29	0.00	52.75	68.78	94.24	93.34
30	0.00	65.44	73.74	78.50	82.98
31	0.00	62.60	73.68	54.14	84.72
32	0.00	61.43	116.20	100.07	100.05

33	0.00	66.48	105.96	80.53	70.57
34	0.00	64.72	99.10	86.29	89.05
35	0.00	65.04	80.37	92.80	100.23
36	0.00	63.60	96.06	99.28	102.53
37	0.00	68.46	106.71	96.92	97.12
38	0.00	62.30	94.83	100.75	104.68
39	0.00	67.49	103.79	88.86	87.16
40	0.00	65.81	83.25	78.73	74.91
41	0.00	63.21	70.99	89.17	107.56
42	0.00	66.53	101.76	92.35	92.32
43	0.00	64.17	85.09	102.96	114.23
44	0.00	68.53	107.44	102.17	102.84
45	0.00	58.76	88.65	92.38	88.82
46	0.00	70.15	123.55	100.71	97.79
47	0.00	68.19	114.25	115.03	114.20
48	0.00	67.57	102.60	93.88	92.88
49	0.00	66.46	110.82	111.29	113.45
50	0.00	69.64	115.98	111.57	117.46
AVG	0.00	64.18	87.54	85.04	93.58
STD	0.00	3.91	21.66	17.32	10.49

Table 4-3: Door Width Results for Test #2.

Run #	Door Width at t=0s (m)	Door Width at t=30s (m)	Door Width at t=60s (m)	Door Width at t=90s (m)	Door Width at t=120s (m)
1	1.01	0.39	0.43	0.36	0.53
2	1.20	1.13	0.92	0.54	0.69
3	0.54	0.46	0.74	0.67	0.98
4	0.97	0.73	0.82	0.62	0.88
5	0.78	0.48	0.17	0.27	0.65
6	0.12	0.15	0.12	0.32	0.54
7	1.17	0.60	0.78	0.61	0.79
8	1.14	0.19	0.12	0.38	0.66
9	0.92	0.31	0.12	0.35	0.66
10	0.53	0.12	0.53	0.49	0.65
11	0.94	0.71	0.76	0.51	0.66
12	0.69	0.21	0.12	0.36	0.63
13	0.64	0.69	0.73	0.45	0.56
14	0.88	0.49	0.18	0.25	0.52

15	0.89	0.26	0.12	0.41	0.83
16	0.58	0.51	0.75	0.54	0.68
17	0.63	0.34	0.53	0.39	0.48
18	0.71	0.29	0.14	0.29	0.50
19	0.80	0.23	0.41	0.43	0.64
20	1.18	0.83	0.78	0.51	0.69
21	1.20	0.78	0.76	0.53	0.72
22	0.61	0.27	0.33	0.34	0.62
23	1.07	0.68	0.88	0.69	0.91
24	1.02	0.19	0.12	0.37	0.66
25	1.11	0.89	1.00	0.69	0.89
26	0.64	0.21	0.12	0.37	0.63
27	1.03	0.76	0.70	0.43	0.55
28	0.72	0.42	0.56	0.44	0.61
29	0.12	0.12	0.63	0.55	0.69
30	1.02	0.38	0.47	0.38	0.54
31	0.75	0.40	0.12	0.30	0.57
32	0.50	0.88	0.95	0.63	0.82
33	0.94	0.78	0.63	0.32	0.38
34	0.93	0.66	0.64	0.46	0.64
35	0.99	0.44	0.66	0.58	0.82
36	0.83	0.61	0.83	0.65	0.86
37	1.16	0.78	0.86	0.59	0.77
38	0.69	0.59	0.84	0.67	0.90
39	1.14	0.74	0.74	0.47	0.61
40	1.05	0.47	0.52	0.33	0.43
41	0.87	0.33	0.56	0.63	0.95
42	1.11	0.70	0.76	0.53	0.69
43	0.92	0.48	0.80	0.76	1.09
44	1.16	0.79	0.94	0.68	0.87
45	0.51	0.50	0.72	0.50	0.61
46	1.10	1.11	1.03	0.63	0.79
47	1.08	0.88	1.19	0.87	1.10
48	1.20	0.72	0.80	0.54	0.70
49	0.93	0.81	1.10	0.83	1.08
50	1.20	0.92	1.13	0.88	1.17
AVG	0.88	0.55	0.61	0.51	0.72
STD	0.26	0.26	0.31	0.16	0.18

Test #3 Results

Table 4-4: HRR results for Test #3.

Run #	HRR at t=0s (kW)	HRR at t=30s (kW)	HRR at t=60s (kW)	HRR at t=90s (kW)	HRR at t=120s (kW)
1	0.00	62.35	99.15	95.78	94.24
2	0.00	64.97	106.66	90.65	91.71
3	0.00	61.15	100.51	94.25	90.36
4	0.00	66.28	108.60	97.91	98.13
5	0.00	63.07	104.83	90.80	87.98
6	0.00	61.75	103.25	102.93	94.91
7	0.00	65.08	107.42	95.76	94.49
8	0.00	63.67	105.04	100.91	101.37
9	0.00	63.81	106.20	98.66	94.68
10	0.00	62.22	97.40	102.35	103.54
11	0.00	63.48	106.26	92.62	89.32
12	0.00	62.79	104.76	97.54	93.72
13	0.00	64.48	105.46	95.35	94.89
14	0.00	65.00	107.62	98.89	98.30
15	0.00	63.85	106.46	100.26	100.55
16	0.00	64.20	103.17	95.21	95.49
17	0.00	62.30	103.61	94.80	93.25
18	0.00	61.81	90.96	101.19	102.84
19	0.00	61.72	92.85	100.73	96.77
20	0.00	65.05	105.83	89.63	84.04
21	0.00	67.38	111.81	91.56	90.49
22	0.00	61.89	91.70	94.26	93.45
23	0.00	62.06	100.38	87.89	85.68
24	0.00	62.69	99.73	98.90	98.29
25	0.00	63.05	100.68	90.91	93.22
26	0.00	62.22	91.92	100.04	94.15
27	0.00	63.84	101.18	95.06	96.11
28	0.00	62.13	100.93	97.37	98.25
29	0.00	65.31	105.54	93.79	93.77
30	0.00	60.95	88.91	94.68	94.36
31	0.00	71.94	75.40	82.75	114.85
32	0.00	62.76	97.82	96.16	98.02
33	0.00	60.23	90.44	97.20	96.58
34	0.00	65.43	108.71	94.77	92.85

35	0.00	61.80	91.79	95.09	95.62
36	0.00	64.12	98.65	92.09	94.75
37	0.00	62.90	97.89	92.13	90.45
38	0.00	62.24	98.35	95.82	95.93
39	0.00	65.25	104.52	86.91	89.42
40	0.00	62.41	98.57	90.55	89.29
41	0.00	63.57	101.39	87.21	89.18
42	0.00	62.91	101.69	86.99	89.28
43	0.00	62.76	94.03	96.55	93.43
44	0.00	62.90	99.88	94.39	98.95
45	0.00	61.25	96.92	100.00	102.57
46	0.00	60.66	91.04	98.05	102.89
47	0.00	62.89	99.71	97.74	96.40
AVG	0.00	63.33	100.12	95.00	95.08
STD	0.00	1.99	6.75	4.48	5.34

Table 4-5: Door width results for Test #3.

Run #	Door Width at t=0s (m)	Door Width at t=30s (m)	Door Width at t=60s (m)	Door Width at t=90s (m)	Door Width at t=120s (m)
1	0.63	0.65	0.74	0.57	0.68
2	0.64	0.77	0.70	0.51	0.67
3	0.58	0.65	0.74	0.53	0.65
4	0.66	0.80	0.80	0.61	0.74
5	0.62	0.71	0.71	0.49	0.61
6	0.62	0.68	0.87	0.61	0.68
7	0.67	0.77	0.80	0.57	0.68
8	0.64	0.73	0.84	0.66	0.79
9	0.64	0.74	0.83	0.59	0.68
10	0.64	0.62	0.84	0.69	0.83
11	0.64	0.74	0.74	0.51	0.64
12	0.62	0.71	0.80	0.57	0.68
13	0.66	0.74	0.77	0.57	0.70
14	0.64	0.77	0.84	0.62	0.74
15	0.62	0.74	0.83	0.64	0.77
16	0.66	0.71	0.74	0.57	0.71
17	0.62	0.69	0.74	0.55	0.68
18	0.66	0.56	0.81	0.67	0.80
19	0.64	0.57	0.81	0.61	0.71

20	0.67	0.76	0.71	0.45	0.56
21	0.67	0.86	0.73	0.51	0.65
22	0.66	0.55	0.71	0.55	0.68
23	0.66	0.66	0.66	0.45	0.58
24	0.66	0.66	0.80	0.62	0.74
25	0.68	0.67	0.68	0.53	0.67
26	0.68	0.57	0.81	0.58	0.68
27	0.64	0.68	0.74	0.58	0.71
28	0.62	0.66	0.77	0.61	0.74
29	0.66	0.76	0.74	0.55	0.68
30	0.61	0.52	0.72	0.56	0.68
31	0.71	0.54	0.61	0.63	0.96
32	0.63	0.63	0.74	0.60	0.74
33	0.59	0.53	0.74	0.59	0.71
34	0.64	0.80	0.77	0.55	0.68
35	0.64	0.56	0.72	0.57	0.71
36	0.66	0.66	0.69	0.55	0.71
37	0.68	0.63	0.71	0.51	0.65
38	0.64	0.64	0.74	0.58	0.71
39	0.66	0.74	0.65	0.47	0.64
40	0.65	0.64	0.68	0.49	0.63
41	0.64	0.69	0.64	0.47	0.63
42	0.64	0.69	0.64	0.47	0.63
43	0.68	0.60	0.74	0.56	0.68
44	0.64	0.66	0.71	0.59	0.77
45	0.60	0.61	0.80	0.66	0.80
46	0.64	0.55	0.74	0.64	0.82
47	0.64	0.66	0.80	0.59	0.71
AVG	0.64	0.67	0.75	0.57	0.70
STD	0.02	0.08	0.06	0.06	0.07

Test #4 Results

Table 4-6: HRR results for Test #4.

Run #	HRR at t=0s (kW)	HRR at t=30s (kW)	HRR at t=60s (kW)	HRR at t=90s (kW)	HRR at t=120s (kW)
1	0.00	59.91	61.01	61.30	52.67
2	0.00	60.31	60.59	61.40	52.74

3	0.00	59.87	61.04	61.30	52.72
4	0.00	60.19	60.69	61.37	52.68
5	0.00	60.30	60.56	61.40	52.65
6	0.00	60.20	60.69	61.36	52.72
7	0.00	60.33	60.40	61.45	52.69
8	0.00	60.13	60.72	61.37	52.64
9	0.00	60.08	60.82	61.34	52.68
10	0.00	60.25	60.63	61.38	52.64
11	0.00	60.07	60.84	61.34	52.66
12	0.00	59.90	61.02	61.30	52.71
13	0.00	59.87	61.05	61.31	52.67
14	0.00	60.23	60.67	61.37	52.70
15	0.00	59.94	60.98	61.31	52.61
16	0.00	60.01	60.91	61.33	52.73
17	0.00	60.31	60.58	61.39	52.70
18	0.00	59.91	60.99	61.32	52.61
19	0.00	59.93	60.98	61.31	52.70
20	0.00	60.27	60.61	61.42	52.72
21	0.00	60.10	60.82	61.35	52.63
22	0.00	59.93	61.01	61.31	52.61
23	0.00	60.26	60.62	61.40	52.69
24	0.00	60.22	60.64	61.38	52.72
25	0.00	60.08	60.83	61.34	52.79
26	0.00	59.87	61.05	61.30	52.77
27	0.00	60.33	60.52	61.51	52.70
28	0.00	60.25	60.62	61.56	52.77
29	0.00	59.88	61.05	61.30	52.69
30	0.00	60.11	60.80	61.35	52.60
AVG	0.00	60.10	60.80	61.35	52.69
STD	0.00	0.16	0.19	0.04	0.05

Test #5 Results

Table 4-7: HRR results for Test #5.

Run #	HRR at t=0s (kW)	HRR at t=30s (kW)	HRR at t=60s (kW)	HRR at t=90s (kW)	HRR at t=120s (kW)
1	0.00	59.55	59.36	60.10	54.01
2	0.00	61.39	64.55	59.05	54.42

3	0.00	59.02	53.46	60.96	54.53
4	0.00	59.73	58.12	60.84	54.32
5	0.00	60.06	61.15	60.51	55.20
6	0.00	59.81	59.22	59.25	54.10
7	0.00	55.89	58.68	61.54	54.27
8	0.00	60.34	71.17	56.30	53.75
9	0.00	60.49	65.51	57.85	53.45
10	0.00	58.25	63.21	61.14	45.35
11	0.00	59.91	65.03	60.04	45.41
12	0.00	58.13	54.96	60.63	55.90
13	0.00	58.71	56.51	63.51	45.51
14	0.00	55.94	58.59	62.11	55.99
15	0.00	59.52	61.06	61.84	45.31
16	0.00	58.54	55.89	62.54	52.87
17	0.00	59.73	66.14	57.75	53.70
18	0.00	59.91	60.63	61.25	52.10
19	0.00	59.75	65.43	59.90	47.09
20	0.00	60.52	50.94	60.83	55.13
21	0.00	59.51	59.72	62.01	51.85
22	0.00	56.07	55.79	61.40	55.62
23	0.00	56.57	54.92	61.64	54.44
24	0.00	60.97	56.47	62.67	48.21
25	0.00	59.81	51.45	60.51	55.49
26	0.00	60.51	72.05	56.22	54.55
27	0.00	59.73	57.93	62.33	47.27
28	0.00	61.05	70.46	56.43	52.99
29	0.00	59.22	66.77	58.18	54.18
30	0.00	60.00	66.55	58.58	53.29
31	0.00	60.00	67.07	58.19	52.80
32	0.00	60.18	57.57	61.37	52.53
33	0.00	55.93	57.85	61.64	52.75
34	0.00	60.15	62.80	59.15	53.59
35	0.00	60.14	63.83	59.34	53.17
36	0.00	57.33	65.95	60.05	47.34
37	0.00	57.69	66.98	59.42	47.14
38	0.00	59.64	65.93	58.38	52.97
39	0.00	60.45	63.29	59.35	52.93
40	0.00	55.37	64.22	59.22	53.71
41	0.00	60.18	65.92	57.71	54.32
42	0.00	55.72	60.99	60.86	52.19
43	0.00	56.34	55.11	62.29	53.03

44	0.00	55.80	59.75	61.92	54.79
45	0.00	57.13	71.32	56.95	53.47
46	0.00	55.85	59.32	62.87	47.87
47	0.00	55.90	57.94	61.76	54.46
48	0.00	59.43	65.80	59.77	45.46
49	0.00	60.00	63.38	58.23	54.35
50	0.00	60.18	53.97	59.40	56.37
AVG	0.00	58.81	61.57	60.13	52.23
STD	0.00	1.78	5.19	1.85	3.27

Table 4-8: Door width results for Test #5.

Run #	Door Width at t=0s (m)	Door Width at t=30s (m)	Door Width at t=60s (m)	Door Width at t=90s (m)	Door Width at t=120s (m)
1	0.76	0.43	1.02	0.32	0.90
2	1.05	0.69	1.20	0.36	0.99
3	1.19	0.12	0.71	0.12	0.91
4	0.85	0.41	1.00	0.37	0.91
5	0.80	0.50	1.20	0.41	1.08
6	0.84	0.44	0.95	0.13	0.87
7	0.12	0.12	1.01	0.35	0.88
8	0.69	0.96	1.20	0.15	0.91
9	0.71	0.67	1.20	0.16	0.82
10	0.62	0.48	1.20	0.14	0.12
11	0.61	0.61	1.20	0.16	0.12
12	0.93	0.12	0.76	0.18	1.17
13	1.15	0.12	1.13	0.15	0.12
14	0.12	0.12	1.06	0.42	1.17
15	0.73	0.47	1.20	0.14	0.12
16	0.12	0.12	0.93	0.35	0.68
17	0.59	0.64	1.20	0.15	0.87
18	0.74	0.49	1.20	0.28	0.70
19	0.59	0.62	1.20	0.12	0.30
20	1.13	0.12	0.60	0.12	1.01
21	0.78	0.44	1.19	0.34	0.66
22	0.12	0.12	0.80	0.17	1.09
23	0.12	0.12	0.76	0.13	0.89
24	1.11	0.42	1.06	0.12	0.35
25	1.20	0.12	0.60	0.12	1.07

26	0.71	1.03	1.20	0.20	1.05
27	0.89	0.41	1.10	0.12	0.30
28	0.77	1.01	1.20	0.12	0.81
29	0.57	0.64	1.20	0.25	0.96
30	0.66	0.68	1.20	0.32	0.83
31	0.62	0.70	1.20	0.18	0.80
32	1.07	0.42	1.03	0.32	0.72
33	0.12	0.12	0.98	0.16	0.69
34	0.77	0.56	1.20	0.30	0.86
35	0.69	0.58	1.20	0.34	0.81
36	0.52	0.51	1.20	0.12	0.30
37	0.55	0.56	1.20	0.12	0.30
38	0.59	0.63	1.20	0.16	0.79
39	0.77	0.59	1.20	0.32	0.75
40	0.12	0.12	1.20	0.12	0.82
41	0.66	0.66	1.19	0.17	0.98
42	0.12	0.12	1.20	0.16	0.65
43	0.12	0.12	0.82	0.15	0.72
44	0.12	0.12	1.13	0.40	0.98
45	0.33	0.69	1.20	0.12	0.83
46	0.12	0.12	1.20	0.12	0.31
47	0.12	0.12	0.97	0.35	0.91
48	0.58	0.61	1.20	0.18	0.12
49	0.75	0.55	1.19	0.16	0.97
50	1.20	0.36	0.64	0.12	1.20
AVG	0.62	0.43	1.08	0.21	0.74
STD	0.34	0.26	0.18	0.10	0.31

Test #6 Results

Table 4-9: HRR results for Test #6.

Run #	HRR at t=0s (kW)	HRR at t=30s (kW)	HRR at t=60s (kW)	HRR at t=90s (kW)	HRR at t=120s (kW)
1	0.00	62.64	66.01	59.76	55.41
2	0.00	61.90	71.25	57.20	54.84
3	0.00	62.23	67.69	58.57	54.92
4	0.00	61.95	70.23	57.39	54.85
5	0.00	62.68	66.21	58.87	54.96

6	0.00	62.90	66.00	59.90	55.02
7	0.00	62.02	69.18	58.33	54.87
8	0.00	62.26	67.99	58.47	54.89
9	0.00	62.76	66.19	60.17	55.04
10	0.00	61.89	71.27	57.23	54.80
11	0.00	62.75	66.16	60.24	54.90
12	0.00	62.59	66.39	59.69	55.03
13	0.00	62.26	67.53	59.56	54.99
14	0.00	62.40	67.11	59.88	54.99
15	0.00	62.26	67.89	59.40	54.92
16	0.00	62.80	66.18	60.16	54.97
17	0.00	62.17	68.37	57.94	54.91
18	0.00	62.38	67.13	59.85	54.91
19	0.00	62.78	66.21	60.00	55.00
20	0.00	62.24	67.92	58.13	54.84
21	0.00	62.20	67.89	59.28	54.95
22	0.00	62.76	65.85	60.42	55.00
23	0.00	62.63	66.24	59.83	55.01
24	0.00	62.72	65.48	63.90	54.76
25	0.00	62.20	67.95	58.48	54.90
26	0.00	62.57	66.42	59.96	54.93
27	0.00	62.93	65.77	60.23	54.95
28	0.00	62.71	66.27	59.66	54.99
29	0.00	62.22	67.84	58.59	53.88
30	0.00	62.02	68.98	57.72	54.91
31	0.00	62.18	67.90	59.62	54.97
32	0.00	62.90	65.57	60.33	54.98
33	0.00	61.99	69.12	57.64	54.89
34	0.00	61.84	72.24	57.02	54.79
35	0.00	61.88	71.66	57.81	54.80
36	0.00	62.90	65.49	60.80	54.97
37	0.00	62.23	67.78	58.63	54.91
38	0.00	62.26	67.48	59.38	55.00
39	0.00	62.70	66.23	59.80	55.05
40	0.00	62.32	67.26	59.68	54.95
41	0.00	62.59	66.33	59.72	55.02
42	0.00	61.95	69.07	58.22	54.92
43	0.00	61.95	69.98	57.46	54.84
44	0.00	62.24	67.59	59.41	54.97
45	0.00	62.24	67.85	58.12	54.95
46	0.00	62.42	66.81	59.57	55.02

47	0.00	62.87	66.02	60.26	54.98
48	0.00	61.87	71.75	57.04	54.82
49	0.00	61.80	69.99	58.15	54.83
50	0.00	62.90	66.01	60.18	54.98
AVG	0.00	62.43	67.39	59.29	54.91
STD	0.00	0.32	1.56	1.31	0.22

Table 4-10: Door width results for Test #6.

Run #	Door Width at t=0s (m)	Door Width at t=30s (m)	Door Width at t=60s (m)	Door Width at t=90s (m)	Door Width at t=120s (m)
1	1.20	1.19	1.20	0.45	0.92
2	1.20	1.18	1.20	0.38	0.92
3	1.20	1.19	1.20	0.41	0.92
4	1.19	1.20	1.20	0.38	0.92
5	1.20	1.19	1.20	0.41	0.92
6	1.20	1.19	1.20	0.45	0.92
7	1.20	1.19	1.20	0.41	0.92
8	1.19	1.19	1.20	0.41	0.92
9	1.20	1.19	1.20	0.45	0.92
10	1.19	1.18	1.20	0.38	0.92
11	1.20	1.19	1.20	0.46	0.92
12	1.20	1.19	1.20	0.45	0.92
13	1.20	1.18	1.20	0.45	0.92
14	1.20	1.19	1.20	0.45	0.92
15	1.19	1.20	1.20	0.45	0.91
16	1.20	1.20	1.20	0.45	0.91
17	1.20	1.20	1.20	0.38	0.92
18	1.20	1.19	1.20	0.45	0.92
19	1.20	1.20	1.20	0.45	0.92
20	1.20	1.19	1.20	0.38	0.91
21	1.20	1.19	1.20	0.45	0.91
22	1.20	1.19	1.20	0.46	0.92
23	1.20	1.19	1.20	0.45	0.92
24	1.20	1.20	1.20	0.68	0.91
25	1.20	1.19	1.20	0.41	0.92
26	1.20	1.20	1.20	0.45	0.91
27	1.20	1.19	1.20	0.45	0.92
28	1.20	1.20	1.20	0.45	0.91
29	1.19	1.19	1.20	0.37	0.90

30	1.20	1.19	1.20	0.38	0.92
31	1.20	1.19	1.20	0.45	0.92
32	1.20	1.19	1.20	0.45	0.91
33	1.20	1.19	1.20	0.38	0.92
34	1.20	1.20	1.20	0.38	0.92
35	1.19	1.18	1.20	0.41	0.92
36	1.20	1.19	1.20	0.49	0.91
37	1.20	1.19	1.20	0.41	0.92
38	1.20	1.18	1.20	0.45	0.92
39	1.20	1.19	1.20	0.45	0.92
40	1.20	1.19	1.20	0.45	0.91
41	1.20	1.19	1.20	0.45	0.92
42	1.19	1.19	1.20	0.41	0.92
43	1.19	1.19	1.20	0.38	0.92
44	1.20	1.19	1.20	0.45	0.91
45	1.20	1.19	1.20	0.38	0.92
46	1.20	1.18	1.20	0.45	0.92
47	1.20	1.19	1.20	0.45	0.92
48	1.19	1.19	1.20	0.38	0.92
49	1.19	1.18	1.20	0.41	0.92
50	1.20	1.19	1.20	0.45	0.92
AVG	1.20	1.19	1.20	0.43	0.92
STD	0.00	0.00	0.00	0.05	0.00

Appendix C Octave Code

IFM "run" file

```
%%Directory Managment
currentDir = pwd;
addpath(strcat(currentDir,'\BRI'))
addpath(strcat(currentDir,'\GA_Files'))

outputDir = [currentDir,'\',timeStamp];
resultsCSVFile = [outputDir,'\Results.csv'];
solCSVFile = [outputDir,'\Final_Solutions.csv'];
mkdir(outputDir);
resultsFID = fopen(resultsCSVFile,'w');
solFID = fopen(solCSVFile,'w');

%% Define a few globals that we'll eventually get rid of
global BRIData;
global fireInformation;
global simulationTime = 176;
global truthData;


%%Global Properties
numRuns = 20;

%Define bounds for HRR
HRR_Max = 2500;
HRR_Min = 5;

%GA Parameters
popSize=700;
numGenerations=50;

boundaryMutationRate=0.06;
multiNonUnifMutationRate=0.16;
nonUnifMutationRate=0.12;
unifMutationRate=0.12;
mutatePointRate=0.12;
arithXoverRate = 0.08;
heuristicXoverRate = 0.08;
simpleXoverRate = 0.2;

normGeomSelectTerm = 0.04; %was 0.08 ???
```

```
BRIData.floorHeights = [2.0];
BRIData.startHRR = 1; %This will be computed automagically below, leave it alone.

%% Create the FIRE ROOM
fireRoom.Name = 'FIRE ROOM';
fireRoom.floorNumber = 1;
fireRoom.startHeight=0;
fireRoom.endHeight=2.0;
fireRoom.floorMaterial=1;
fireRoom.ceilingMaterial=1;
fireRoom.length=1.9;
fireRoom.width=2.5;


fireVent1.Room = 'HALL ROOM';
fireVent1.width = 1.2;
fireVent1.height = 2.0;
fireVent1.widthVaries  = true;
fireVent1.heightVaries = false;
fireVent1.minWidth=0.1; %Fractions of the actual width
fireVent1.maxWidth=1.0; %Fractions of the actual width

fireRoom.vents = [fireVent1];

%% Create the HALL Room
hallRoom.Name = 'HALL ROOM';
hallRoom.floorNumber = 1;
hallRoom.startHeight=0;
hallRoom.endHeight=2.0;
hallRoom.floorMaterial=2;
hallRoom.ceilingMaterial=2;
hallRoom.length=3.7;
hallRoom.width=1.1;

hallVent1.Room = 'COLD ROOM';
hallVent1.width  = 0.6;
hallVent1.height = 2.0;
hallVent1.widthVaries  = false;
hallVent1.heightVaries = false;
hallVent1.minWidth=0.1; %Fractions of the actual width
hallVent1.maxWidth=1.0; %Fractions of the actual width

hallRoom.vents = [hallVent1];

%% Create the COLD ROOM
coldRoom.Name = 'COLD ROOM';
```

```
coldRoom.floorNumber=1;
coldRoom.startHeight=0;
coldRoom.endHeight=2;
coldRoom.floorMaterial=2;
coldRoom.ceilingMaterial=2;
coldRoom.length=1.8;
coldRoom.width=2.5;

coldRoomVent.Room = 'Outside';
coldRoomVent.width=0.1;
coldRoomVent.height=2.0;
coldRoomVent.widthVaries  = false;
coldRoomVent.heightVaries = false;
coldRoomVent.minWidth=0.1; %Fractions of the actual width
coldRoomVent.maxWidth=1.0; %Fractions of the actual width


coldRoom.vents = [coldRoomVent];

%% Combine all your room objects here
BRIData.rooms = [fireRoom,hallRoom,coldRoom];

%% Create the Fire Information Object
fireInformation.room = 'FIRE ROOM';
fireInformation.fuel  = 4;
fireInformation.airTemperature = 22.0;
fireInformation.humidity = 50.0;
fireInformation.time = [0,30,60,90,120];
fireInformation.HRR  = zeros(1,length(fireInformation.time));

truthData.rooms(1).Name = 'FIRE ROOM';
truthData.rooms(1).tempTime = [];
truthData.rooms(1).temp = [];
truthData.rooms(1).heightTime = [];
truthData.rooms(1).height = [];
[truthData.rooms(1).tempTime,truthData.rooms(1).temp] = textread('fireroom.dat','%f
%f');
[truthData.rooms(1).heightTime,truthData.rooms(1).height] =
textread('smokeheight.dat','%f %f');



Bounds = [];

%% Define bounds for vents that have varying widths
for i = 1:length(BRIData.rooms)
```

```
  for j = 1:length(BRIData.rooms(i).vents)
     currentVent = BRIData.rooms(i).vents(j);
     if currentVent.widthVaries == 1

                  for k = 1:length(fireInformation.time)
                        Bounds = [Bounds;currentVent.minWidth,currentVent.maxWidth];

                  end
                  BRIData.startHRR = BRIData.startHRR + length(fireInformation.time);
     end
  end
end



for i = 1:length(fireInformation.time)
  Bounds = [Bounds;HRR_Min,HRR_Max];
end

fprintf(resultsFID,'%i\r\n', numRuns)
fprintf(resultsFID,'%i\r\n', length(BRIData.rooms))

fclose(resultsFID);
fclose(solFID);


numTimeSteps=4;
global totalTimes       = [[], [], [], []]

% Create the initial population
createInitPop=1;
if exist('initPop')
  str = input('Do you want to create a new initial population? (Y\N): ' ,'s');
  if strcmp(str,'Y') != 1
    createInitPop=0;
  end
end

if createInitPop == 1
  disp('Creating initial population.')
  initPop=initializega(popSize,Bounds,'evalFitness',[]);
else
  disp('Using last initial population.')
end

for currentRun = 1:numRuns
```

```
  totalTimes       = [[], [], [], []];

  resultsFID = fopen(resultsCSVFile,'a');
  solFID = fopen(solCSVFile,'a');

  disp(['Beginning Run ', num2str(currentRun), '.'])

  %% Start Running the GA
  disp('Starting GA')
  disp(['Running ', num2str(numGenerations), ' generations.'])
  disp(['Population Size: ', num2str(popSize)])
  [12 0 0;18 numGenerations 3;12 numGenerations 3;12 0 0];
  mutOps=[boundaryMutationRate*popSize 0 0;multiNonUnifMutationRate*popSize
numGenerations 3; nonUnifMutationRate*popSize numGenerations
3;unifMutationRate*popSize 0 0; mutatePointRate*popSize 0 0];
  xOverOps=[arithXoverRate*popSize 0;heuristicXoverRate*popSize
3;simpleXoverRate*popSize 0];
  [bestSol endPop bPop trace] = ga(Bounds,'evalFitness',[],initPop,[1e-6 1
0],'maxGenTerm',numGenerations,['normGeomSelect'],[normGeomSelectTerm],['arithXo
ver heuristicXover simpleXover'],xOverOps,['boundaryMutation multiNonUnifMutation
nonUnifMutation unifMutation'],mutOps);

  writeResultsToCSV(bestSol, length(BRIData.rooms), resultsFID,1)
  writeResultsToCSV(bestSol, length(BRIData.rooms), solFID, 0)

  %Render plots and save them off
  close all;
  for i = 1:length(truthData.rooms)
    close all;
        plotHandle1 = figure(1);
    hold on;

    %Plot the truth data according to the experiment
    title([truthData.rooms(i).Name, ' Temperature Plot'])
    plot(truthData.rooms(i).tempTime,truthData.rooms(i).temp,'r')

    %Plot the generated's solution temperature curve
    evalFitness(bestSol,[]);
    [BRITime,BRITempData, BRIHeightData] = loadBRITempData();
    plot(BRITime,BRITempData(:,i),'b');
    legend('Experimental Data', 'Best Solution')

    filename = ['\Run_',num2str(currentRun), '_', truthData.rooms(i).Name,
'_Temp_Plot.png'];
    filename = strrep(filename,' ','_');
        filename = [outputDir,filename]
```

```
    saveas(plotHandle1,filename,'png')

        plotHandle2 = figure(2);
        hold on;
    title([truthData.rooms(i).Name, ' Height Plot'])
    plot(truthData.rooms(i).heightTime,truthData.rooms(i).height,'r')

    %Plot the generated's solution temperature curve
    plot(BRITime,BRIHeightData(:,i),'b');
    legend('Experimental Data', 'Best Solution')

    filename = ['\Run_',num2str(currentRun), '_', truthData.rooms(i).Name,
'_Height_Plot.png'];
    filename = strrep(filename,' ','_');
        filename = [outputDir,filename]
    saveas(plotHandle2,filename,'png')
  end


  fid = fopen(strcat('Profile_Time_',num2str(currentRun), '.txt'),'w');
  for k = 1:numTimeSteps
    averageTime = mean(totalTimes(k));
    fprintf(fid,'Step %i: %10.10f\n',k,averageTime);
  end

  fclose(fid);
        fclose(resultsFID);
        fclose(solFID);
end
```

EvalFitness Function

```
function [sol, val] = evalFitness(sol,options)
  %% DEFINE THIS FUNCTION IN MORE DETAIL HERE

  val = 0;

  global BRIData;
  global fireInformation;
  global simulationTime;
  global truthData;

  global totalTimes;

  numPoints = length(fireInformation.time);

  %Some number of points in our solution represent the varying vent sizes. For each vent
that varies there are a number of points in the solution that represent its width (as a
fraction of it's actual width from 0.0 to 1.0)
  ventIndex=1;
  startTime=time;
  for i = 1:length(BRIData.rooms)
    for j = 1:length(BRIData.rooms(i).vents)
      currVent = BRIData.rooms(i).vents(j);
      if currVent.widthVaries == true
        %If we found a vent whose width varies, grab it's various widths over time
        BRIData.rooms(i).vents(j).widthsOverTime = sol((ventIndex-
1)*numPoints+1:(ventIndex)*numPoints);
        ventIndex = ventIndex+1;
      end
    end
  end

  step1Time=time-startTime;

  %Some number of points in our solution represent the actual HRR. We get the starting
index for that from the BRIData object.
  startTime=time;
  startHRR = BRIData.startHRR;
  sol(startHRR)=0;
  for i = 0:numPoints-1
    fireInformation.HRR(i+1) = sol(i+startHRR);
  end
  writeBRIData('BRI/inp.dat',BRIData,fireInformation,simulationTime);
  step2Time = time-startTime;
```

```
  cd('BRI')

  startTime=time;
  [status,output]=system('BRI2002-E.exe > out.txt 2>&1');
  step3Time = time-startTime;
  cd('../')


  startTime=time;
  step4Time=-1;
  if status != 0
    val = -100000;
    fprintf('F')
  else
          %disp('BRI Passed.')

    %Loads the temperature data the BRI output from all rooms.
    %Time contains each point of time from the BRI output.
    %Note that this needs to be in 1 second increments from 0:simulationTime
    %tempData is a matrix where row is time and column is room number
    [times,tempData,heightData] = loadBRITempData();
    if times(length(times)) != simulationTime
      val=-1000000;
      fprintf('F');
    else
      fprintf('P');

      numTruthPoints = length(truthData.rooms);
      %Loop through all of the truth data sets we have (one per room, if a room is
missing data truth data that is fine).

      val = 0;
      for i = 1:numTruthPoints
        %get the room number our current set of truth data is associated with
        roomIndex = getRoomIndex(BRIData.rooms,truthData.rooms(i).Name);
        currentRoomBRITempData = tempData(:,roomIndex);
        currentRoomBRIHeightData = heightData(:,roomIndex);

        %Index the BRI data for the current room with the truth data's time
      currentRoomBRITempData_TruthDataTime =
currentRoomBRITempData(int32(truthData.rooms(i).tempTime+1));
      deltaFunc = currentRoomBRITempData_TruthDataTime-truthData.rooms(i).temp;
      val = val + sum(abs(deltaFunc)/simulationTime);

            currentRoomBRIHeightData_TruthDataTime =
currentRoomBRIHeightData(int32(truthData.rooms(i).heightTime+1));
```

```
        deltaFunc = currentRoomBRIHeightData_TruthDataTime-
truthData.rooms(i).height;
        val = (val + sum(abs(deltaFunc)*50)/simulationTime)/2;

        end

        %negative the fitness since a smaller standard deviation means a more fit solution,
but a larger fitness is better.
        val=-val;

        %disp(['Fitness: ',num2str(val)]);
      end
      step4Time = time-startTime;
    end

    %fprintf('\nTest: %i, %i\n', currentGeneration, currentSolution)
    totalTimes(1) = step1Time;
    totalTimes(2) = step2Time;
    totalTimes(3) = step3Time;
    totalTimes(4) = step4Time;

end
```

WriteBRI Function

```
function writeBRIData(file, BRIData, fireInformation, simulationTime)
  %% BRI Data Object
  %% Propreties:
  %%          .fuelType
  %%          .
  %%          .floorHeights
  %%          .Rooms[]
  %%               .Name
  %%               .length
  %%               .width
  %%               .startHeight
  %%               .endHeight
  %%               .Vents[]
  %%                    .ConnectingRoom
  %%                    .VentWidth
  %%                    .VentHeigh
  %%                    .Distance from Floor

  %%Fire Information Object:
  %% Properties:
  %%          .location = Room Name (string)
  %%          .time[] - double
  %%          .


  %Open the file
  fid = fopen(file,'w');

  %Print Arbitary Header
  fprintf(fid,'Compartment_FIRE\r\n2013.11.20\r\n01\r\nSAMPLE_CALCULATION\n');

  %Print Simulation Time Row
  fprintf(fid,['    ', numberPadSpacing(simulationTime,11,1),'1.     100.0       1.0\r\n']);

  %Print Number of floors
  fprintf(fid,['    ',num2str(length(BRIData.floorHeights)),'\r\n']);

  %Write the floor heights row
  fprintf(fid,['      ']);
  for i = 1:length(BRIData.floorHeights)
    fprintf(fid,num2str(BRIData.floorHeights(i)));
  end
  fprintf(fid,['\r\n'])

  %Print the number of rooms row
```

```
  fprintf(fid,['    ', num2str(length(BRIData.rooms)),'\r\n']);

  %Print the Room Label / Properties Row
  for i = 1:length(BRIData.rooms)
    fprintf(fid,'%i %s', i, strPadSpacing(['(',BRIData.rooms(i).Name,')'],22,1));
    fprintf(fid,'1%s%s',numberPadSpacing(BRIData.rooms(i).startHeight,10,0),
numberPadSpacing(BRIData.rooms(i).endHeight,10,0));
    fprintf(fid,'    1%s%s
1\r\n',numberPadSpacing(BRIData.rooms(i).floorMaterial,5,0),
numberPadSpacing(BRIData.rooms(i).ceilingMaterial,5,0));
    fprintf(fid,'%s%s%s\r\n',numberPadSpacing(0.0,10,0),
numberPadSpacing(BRIData.rooms(i).length,10,0),
numberPadSpacing(BRIData.rooms(i).width,10,0))
  end

  ventID=1;
  for i = 1:length(BRIData.rooms)
    for j = 1:length(BRIData.rooms(i).vents)
      fprintf(fid,'%s%s%s',numberPadSpacing(i,4,0),
numberPadSpacing(getRoomIndex(BRIData.rooms,BRIData.rooms(i).vents(j).Room),6,
0), numberPadSpacing(1,5,0))
      fprintf(fid,'%s%s',numberPadSpacing(BRIData.rooms(i).vents(j).width,10,0),
numberPadSpacing(BRIData.rooms(i).vents(j).height,10,0));
      if BRIData.rooms(i).vents(j).widthVaries == true
        fprintf(fid,'%s%s\r\n',numberPadSpacing(0,10,0),
numberPadSpacing(ventID,20,0));
        ventID=ventID+1;
      else
        fprintf(fid,'%s%s\r\n',numberPadSpacing(0,10,0), numberPadSpacing(0,20,0));
      end
    end
  end



  fprintf(fid, ' 9999 \r\n');
  ventID=1;
  for i = 1:length(BRIData.rooms)
    for j = 1:length(BRIData.rooms(i).vents)
      if BRIData.rooms(i).vents(j).widthVaries == true
        %Put Vent/Schedule ID and number of points
        fprintf(fid,'%s%s\n',numberPadSpacing(ventID,5,0),
numberPadSpacing(length(fireInformation.time),5,0))

        %Print out each measurement time
        for k=1:length(fireInformation.time)
```

```
            fprintf(fid,'%s',numberPadSpacing(fireInformation.time(k),10,0))
          end
          fprintf(fid,'\n');

          %Print out vent width for each time
          for k=1:length(fireInformation.time)

fprintf(fid,'%s',numberPadSpacing(BRIData.rooms(i).vents(j).widthsOverTime(k),10,0))
          end
          fprintf(fid,'\n');

          ventID=ventID+1;
        end
      end
    end

    fprintf(fid, ' 9999 \r\n');
    fireRoomIndex = getRoomIndex(BRIData.rooms,fireInformation.room);
    fprintf(fid,'%s\n',numberPadSpacing(fireRoomIndex,5,0));

    %Print out number of measure points we have

fprintf(fid,'%s%s\n',numberPadSpacing(length(fireInformation.time),5,0),numberPadSpa
cing(1,5,0));

    %Print out each measurement time
    for i=1:length(fireInformation.time)
      fprintf(fid,'%s',numberPadSpacing(fireInformation.time(i),10,0))
    end
    fprintf(fid,'\n')

    %Print out measured HRR for each time
    for i=1:length(fireInformation.time)
      fprintf(fid,'%s',numberPadSpacing(fireInformation.HRR(i),10,0))
    end
    fprintf(fid,'\n')

    %Print out for each time (Area of the Fire)
    %fprintf(fid,'%s',numberPadSpacing(0,10,0))
    for i=1:length(fireInformation.time)
      %fprintf(fid,'%s',numberPadSpacing(fireInformation.HRR(i)/625,10,0))
      if fireInformation.HRR(i)/500 < 1.5
        firearea=fireInformation.HRR(i)/500;
      else
        firearea=1.5; %BRI seems to become unstable if the area gets comparable to the
size of the room.
```

```
    end
    fprintf(fid,'%s',numberPadSpacing(firearea,10,0))
  end
  fprintf(fid,'\n')

  %Print out 0's for reasons unnkown
  for i=1:length(fireInformation.time)
    fprintf(fid,'%s',numberPadSpacing(0,10,0))
  end
  fprintf(fid,'\n')

  %Print out fuel type
  fprintf(fid,'%s\r\n',numberPadSpacing(fireInformation.fuel,5,0))

  %Unknown lines
  fprintf(fid,'    1    1\r\n');

  %Print out Fire Rooms Temperature and Humidity

fprintf(fid,'%s%s\r\n',numberPadSpacing(fireInformation.airTemperature,10,0),numberPa
dSpacing(fireInformation.humidity,10,0))

  %Unknown lines
  %Unknown lines
  fprintf(fid,'    2\r\n');
  fprintf(fid,'                INSUL    1       0.9    0.0359 0.0000512     0.902     357.7\r\n');
  fprintf(fid,'                GYPSU    1       0.9    0.0159 0.0001400     0.900     770.0\r\n');
  fprintf(fid,'    1\r\n');
  %Print Outdoor Temperature

fprintf(fid,'%s%s\r\n',numberPadSpacing(fireInformation.airTemperature,10,0),numberPa
dSpacing(fireInformation.humidity,10,0))

  %Unknown lines
  fprintf(fid,'    2\r\n       0.0      0.00      0.00\r\n       0.0       \r\n    0\r\n');

  %Another Marker
  fprintf(fid,' 9999 ')
  fclose(fid);

end
```

Bibliography

[1] J. R. Hall. "The total cost of fire in the United States." National Fire Protection Association Fire Analysis and Research. Available at http://www.nfpa.org/newsandpublications/nfpa-journal/2011/september-october-2011/news-and-analysis/fire-analysis-and-research. Jan 2014.

[2] A. Cowlard, L. Auersperg , J.B. Richon, G. Rein, S. Welch, A. Usmani, J.L. Torero, "A Simple Methodology for Sensor Driven Prediction of Upward Flame Spread", Proceedings of the 5th International Mediterranean Combustion Symposium, Monastir, Tunisia, 9-13. Sep 2007.

[3] C. Lautenberger, G. Rein, C. Fernandez-Pello, "The application of a genetic algorithm to estimate material properties for fire modeling from bench-scale fire test data." Fire Safety Journal. 2005.

[4] W.S. Lee, and S.K. Lee. "The estimation of fire location and heat release rate by using sequential inverse method," Journal of the Chinese Society of Mechanical Engineers. Vol 26, No. 2. pp. 201-207. 2005.

[5] National Institute of Standards and Technology. *FDS-SMV 6.* Available at http://www.nist.gov/el/fire_research/fds_smokeview.cfm. 2014.

[6] W.D. Davis, and G.P. Forney. "A sensor-driven fire model version 1.1,"National Institute of Standards and Technology, NISTIR 6705. Jan 2001.

[7] W.D. Davis. "A sensor-driven fire model version 1.2," National Institute of Standards and Technology, NIST SP 1110. Jul 2010.

[8] S. Koo, et al. "Sensor-linked fire simulation using a Monte-Carlo approach." Fire Safety Science 9:1389-1400, doi:10.3801/IAFSS.FSS.9-1389.

[9] W. Jahn, G. Rein, J.L. Torero. "Data assimilation in enclosure fire dynamics – towards adjoint modelling, Evolutionary and Deterministic Methods for Design, Optimization and Control." T. Burczynski and J. Périaux (Eds.) CIMNE Barcelona, Proceedings of EUROGEN 2009, Cracow, Polad. Jun 2009. http://www.see.ed.ac.uk/~grein/rein_papers/Jahn_Eurogen2009.pdf

[10] L. Han, et al. "FireGrid: An e-infrastructure for next-generation emergency response support." J. Parallel Distrib. Comput. Volume 70, Issue 11, November 2010, Pages 1128-1141 (2010), doi:10.1016/j.jpdc.2010.06.005

[11] Rochoux, M.C., Emery, C., Ricci, S., Cuenot, B., Trouvé, A. (2013) "Towards predictive simulation of wildfire spread at regional scale using ensemble-based data assimilation to correct the fire front position", Fire Safety Science – Proc. Eleventh International Symposium, International Association for Fire Safety Science, submitted for publication.

[12] Rochoux, M.C., Cuenot, B., Ricci, S. and Trouvé, A. (2012) "Towards predictive simulations of wildfire spread using data assimilation and

uncertainty quantification", Proc. 2012 Summer Program, Center for Turbulence Research, Stanford University, California.

[13] Rochoux, M.C., Cuenot, B., Ricci, S., Trouvé, A., Delmotte, B., Massart, S., Paoli, R. and Paugam, R. (2013) "Data assimilation applied to combustion", C.R. Mécanique 341:266-276.

[14] Rochoux, M.C., Delmotte, B., Cuenot, B., Ricci, S. and Trouvé, A. (2013) "Regional-scale simulations of wildland fire spread informed by real-time flame front observations," Proc. Combust. Inst., 34:2641-2647.

[15] A. Neviackas. "Inverse fire modeling to estimate the heat release rate of compartment fires." University of Maryland, Master's Thesis. 2007.

[16] W.D. Walton, and P.H. Thomas. "Estimating Temperatures in Compartment Fires." In *SFPE Handbook of Fire Protection Engineering.* 3rd ed. 2002, pp3-171, 3-188.

[17] G. Ligi. "Analisi sperimentale sul comportamento di sensori ambientali in condizioni di incendio in spazi confinati." Universita di Bologna. Master's thesis. 2011.

[18] National Fire Protection Association. "Standard for Smoke Control Systems." In *NFPA 92*. 2012 edition. pp-92:12-13.

[19] T. Wakamatsu. Ed. "BRI2002: Two layer zone smoke transport model." Fire Science and Technology. Vol 23, No. 1 (Special Issue). 2004.

[20] H.W. Emmons, and T. Tanaka. "Vent Flows." In *SFPE Handbook of Fire Protection Engineering.* 4th ed. 2008, pp2-48.

[21] GNU Octave. "About New Octave." Available at https://www.gnu.org/software/octave/about.html. 2014.